Tcte1 knockout influence on energy chain transportation, apoptosis and spermatogenesis – implications for male infertility

Running title: *Tcte1* gene in male infertility – mouse 'knockout' model

Marta Olszewska[1], Agnieszka Malcher[1], Tomasz Stokowy[2], Nijole Pollock[3], Andrea J. Berman[4], Sylwia Budkiewicz[1], Marzena Kamieniczna[1], Hanna Jackowiak[5], Piotr Jedrzejczak[6], Alexander N. Yatsenko[3], Maciej Kurpisz[1*].

[1] Institute of Human Genetics, Polish Academy of Sciences, Poznan, Poland
[2] Scientific Computing Group, IT Division, University of Bergen, Norway
[3] Department of OB/GYN and Reproductive Sciences, School of Medicine, University of Pittsburgh, PA, USA
[4] Department of Biological Sciences, University of Pittsburgh, PA, USA
[5] Department of Histology and Embryology, Poznan University of Life Sciences, 60-625 Poznan, Poland
[6] Division of Infertility and Reproductive Endocrinology, Department of Gynecology, Obstetrics and Gynecological Oncology, Poznan University of Medical Sciences, 60-535 Poznan, Poland

[*] Corresponding author:

Maciej Kurpisz, PhD, MD
Institute of Human Genetics, Polish Academy of Sciences
Strzeszynska 32
60-479 Poznan, POLAND
phone: +48616579202
e-mail: maciej.kurpisz@igcz.poznan.pl

other authors' emails:

Marta Olszewska, PhD	marta.olszewska@igcz.poznan.pl
Agnieszka Malcher, PhD	agnieszka.malcher@igcz.poznan.pl
Tomasz Stokowy, PhD	tomasz.stokowy@uib.no
Nijole Pollock, BSc	Nijole.pollock@gmail.com
Andrea J. Berman, PhD	AJB190@pitt.edu
Sylwia Budkiewicz, MSc	sylwia.budkiewicz@wp.pl
Marzena Kamieniczna, PhD	marzena.kamieniczna@igcz.poznan.pl
Hanna Jackowiak, PhD	hanna.jackowiak@up.poznan.pl
Piotr Jedrzejczak, PhD, MD	piotrjedrzejczak@gmail.com
Alexander N. Yatsenko, PhD, MD	yatsenkoan@mwri.magee.edu

ORCiD:

Marta Olszewska, PhD	0000- 0002- 2337- 4545
Agnieszka Malcher, PhD	0000- 0002- 3433- 6990
Tomasz Stokowy, PhD	0000-0003-0017-8338
Nijole Pollock, BSc	-
Andrea J. Berman, PhD	0000-0003-1217-7412
Sylwia Budkiewicz, MSc	-
Marzena Kamieniczna, PhD	0000-0002-9619-8220
Hanna Jackowiak, PhD	0000-0001-5167-8215
Piotr Jedrzejczak, PhD, MD	0000-0003-2437-7737
Alexander N. Yatsenko, PhD, MD	0000-0002-1690-0172
Maciej Kurpisz, PhD, MD	0000-0003-3275-3245

Abstract

STUDY QUESTION: Is *Tcte1* mutation causative for male infertility?

SUMMARY ANSWER: Collected data underline the complex and devastating effect of the single-gene mutation on testicular molecular network, leading to male reproductive failure.

WHAT IS KNOWN ALREADY: Latest data revealed mutations in genes related to axonemal dynein arms as causative for morphology and motility abnormalities in spermatozoa of infertile males, including dysplasia of fibrous sheath (DFS) and multiple morphological abnormalities in the sperm flagella (MMAF). The nexin-dynein regulatory complex (N-DRC) coordinates the dynein arm activity, and is built from DRC1-DRC7 proteins. DRC5 (TCTE1) – one of N-DRC element, has been already reported as a candidate for abnormal sperm flagella beating, however, only in restricted manner with no clear explanation of respective observations.

STUDY DESIGN, SIZE, DURATION: Using CRISPR/Cas9 genome editing technique, mouse knockout line of *Tcte1* gene was created on the basis of C57Bl/6J strain. Then, the mouse reproductive potential, semen characteristics, testicular gene expression level, sperm ATP and testis apoptosis level measurements have been performed, followed by visualization of N-DRC proteins in sperm, and protein modeling *in silico*. Also, a pilot genomic sequencing study of samples from human infertile males (n=248) was applied for screening of *TCTE1* variants.

PARTICIPANTS/MATERIALS, SETTING, METHODS: To check the reproductive potential of KO mice, adult animals were crossed for delivery of three litters per caged pair, but no longer than for 6 months, in various combinations of zygosity. All experiments were performed for wild type (WT – control group), heterozygous *Tcte1*$^{+/-}$, and homozygous *Tcte1*$^{-/-}$ male mice. Gross anatomy was performed on testis and epididymis, followed by semen analysis. Sequencing of RNA (RNAseq; Illumina) has been done for mice testis tissues. STRING interactions have been checked for protein-protein interactions, based on changed expression level of corresponding genes identified in the mouse testis RNAseq experiments. Immunofluorescence *in situ* staining was performed to detect the N-DRC complex proteins: Tcte1 (Drc5), Drc7, Fbxl13 (Drc6), and Eps8l1 (Drc3) in mouse spermatozoa. To determine the ATP amount in spermatozoa, the luminescence level was measured. Also, immunofluorescent *in situ* staining was performed to check the level of apoptosis via caspase 3 visualization on mouse testis samples. DNA from whole blood samples of infertile males (n=137 non-obstructive azoospermia or cryptozoospermia, n=111 samples with spectrum of oligoasthenoteratozoospermia, including n=47 with asthenozoospermia) has

been extracted to perform genomic sequencing (WGS, WES or Sanger). Protein prediction modeling of human identified variants and the exon 3 structure deleted in mouse knockout has been also performed.

MAIN RESULTS AND THE ROLE OF CHANCE: No progeny at all was found for homozygous males with revealed oligoasthenoteratozoospermia, while heterozygous animals (fertile) manifested oligozoospermia, suggesting haploinsufficiency. RNA-sequencing of the testicular tissue showed the influence of *Tcte1* mutations on the expression pattern of 21 genes responsible for mitochondrial ATP processing, linked with apoptosis, or spermatogenesis. In *Tcte1*$^{-/-}$ males the protein revealed only residual amounts in sperm head nucleus, and was not transported to sperm flagella, as other N-DRC components. Decreased ATP level (2.4-fold lower) was found in spermatozoa of homozygous mice, together with disturbed tail:midpiece ratio, leading to abnormal sperm tail beating. Casp3-positive signals (indicating apoptosis) were observed in spermatogonia only, at similar level in all three mouse genotypes. Mutation screening of human infertile males revealed 1 novel and 5 ultrarare heterogeneous variants (predicted as disease causing) in 6.05% of patients studied. Protein prediction modeling of identified variants revealed changes in the protein surface charge potential, leading to disruption in helix flexibility or its dynamics, thus, suggesting the disrupted TCTE1 interaction with its binding partners located within the axoneme.

KEYWORDS

TCTE1, *DRC5*, N-DRC, mouse knockout model, male infertility, asthenozoospermia, oligoasthenoteratozoospermia, oligozoospermia, spermatogenesis, sperm motility, sperm mitochondria, mitochondrial respiratory complex, *mt-Co2*, *Fetub*, haploinsufficiency, MMAF, apoptosis

113 **INTRODUCTION**

114 Infertility has been defined by World Health Organization as a social disease concerning approximately
115 10-18% of couples at reproductive age, which are unable to conceive within 1 year of regular unprotected sexual
116 intercourse [WHO, 2020]. Approximately 7% of males and ~12% of females worldwide reveal reproductive
117 problems, while the male factor is responsible for approximately 20-30% of all infertility cases [Barratt *et al.,*
118 2017; Vander Borght and Wyns, 2018; Agarwal et al., 2021]. Male infertility is a disease with multifactorial
119 etiology, including: genetic factors, chromosomal aberrations, epigenetic mutations, hormonal abnormalities,
120 infections or reproductive tract abnormalities [Agarwal et al., 2021; Matzuk and Lamb 2008; Zorrilla and Yatsenko
121 2013; Krausz and Riera-Escamilla 2018]. Genetic causes of male infertility can be detected in ~10-15% of cases,
122 while in 25-50% of infertile males the etiology remains unexplained [Agarwal *et al.,* 2021; Matzuk and Lamb
123 2008; Zorrilla and Yatsenko 2013]. The male infertility phenotype mostly results in decreased semen parameters,
124 including: low sperm concentration, abnormal morphology or diminished motility. The actual standards for
125 genetic testing of male infertility rely on chromosomal screening for structural and numerical abnormalities,
126 followed by analyses of deletions in the AZF (azoospermia factor) regions of the Y chromosome [Hwang et al.,
127 2018]. However, it is still not sufficient due to the fact, that approximately 2,000 genes may be related to
128 spermatogenesis, while only ~10% of them seems to have documented fertility role, so far [Krausz and Riera-
129 Escamilla 2018; Houston *et al.,* 2021] Recent years NGS technology development, including genomic sequencing
130 of DNA (exome or genome; large cohorts of patients), and RNA (RNAseq, scRNAseq on reproductive tissues),
131 followed by animal models of infertility (mostly mouse models; more than 860 genes evaluated, so far [Mouse
132 Genome Informatics, 24 June 2021]) have started the new era of exploration on the massive scale [Houston *et*
133 *al.,* 2021; Oud *et al.,* 2021; Wyrwoll *et al.,* 2020; Hardy *et al.,* 2021; Xavier *et al.,* 2021].

134 Beside the genes related to spermatogenesis and low sperm count, also studies of candidates
135 responsible for diminished sperm motility are pending. Thus, the main structural element responsible for motility
136 – the sperm flagella, has to be of high-quality to guarantee sperm motility and then fertilization success. It is
137 known that mutations in genes encoding factors involved in ciliogenesis process, lead to defects in structure
138 and/or functioning of cilia [Girardet *et al.,* 2019; Sironen *et al.,* 2020; Smith *et al.,* 2021; Kumar and Reiter 2021]
139 There is a plenty of data concerning respiratory cilia, however, still little is known about the axonemal dynein
140 arms functioning in sperm tail. Latest data revealed mutations in genes related to axonemal dynein arms as
141 causative for morphology and motility abnormalities in spermatozoa of infertile males [Girardet *et al.,* 2019;

142 Sironen *et al.,* 2020; Aprea *et al.,* 2021; Lorès *et al.,* 2021; Touré *et al.,* 2021; Martinez *et al.,* 2022]. Two
143 definitions were established: (i) for sperm cells with disorganization in axonemal structures, so called dysplasia
144 of fibrous sheath (DFS) [Chemes *et al.,* 1998] and (ii) for multiple morphological abnormalities in the sperm
145 flagella (MMAF), concerning all possible defects of sperm tail, mainly short and thick flagella, and a lack of the
146 central pair (CP) of microtubules or dynein arms [Khelifa *et al.,* 2014]. Spectrum of abnormal sperm tail
147 phenotypes observed allows qualification of a part of disorders into both listed groups (DFS and MMAF) [Sironen
148 *et al.,* 2020; Touré *et al.,* 2021]

149 The basic structural element of motile cilia and flagella is axoneme built from nine microtubules
150 arranged in doublets positioned radially and one central pair (CP) of singlet microtubules. This central pair is
151 connected to radial spokes (RS) – protein complexes of mechanic regulatory network responsible for regular
152 waveform beating of the cilia [Gui *et al.,* 2019]. RS are linked to inner dynein arms (IDA) localized within each
153 outer dublet. Each outer doublet carries outer dynein arms (ODA) – multi-subunit motor protein complexes,
154 responsible for generation and regulation of sliding between dynein arms leading to ATP-dependent beating
155 [Satir *et al.,* 2014; Wilson et al., 2015]. The 9+2 basic structure is evolutionary conservative [Girardet *et al.,* 2019;
156 Touré *et al.* 2021; Ishikawa 2017]. Doublets are linked with the nexin-dynein regulatory complex (N-DRC), which
157 coordinates the dynein arm activity and stabilizes the attachment of doublet microtubules. The N-DRC is built
158 from DRC1-DRC7 proteins, among which DRC1, DRC2 and DRC4 are responsible for physical linkage between A
159 and B microtubules of doublets [Gui *et al.,* 2019; Morohoshi *et al.,* 2020; Bowar *et al.,* 2018; Wirschell *et al.,*
160 2013]. In terms of male infertility, the best studied gene among N-DRC is *DRC7* (MIM:618769), which is amenable
161 for proper assembly of the N-DRC structure (in *Drc7*$^{-/-}$ male mice the length of the sperm tail was reduced,
162 followed by abnormalities of sperm head morphology) [Morohoshi *et al.,* 2020]. Mouse model of *Drc6* (*Fbxl13*)
163 gene (MIM:609080) revealed no essential role in sperm formation and motility [Morohoshi *et al.*, 2020],
164 however, its disruption together with CEP192 (MIM:616426) leads to defects in HEK293T cell motility [Fung et
165 al., 2018]. Mutations in *Drc3* gene (MIM:618758) indirectly revealed male infertility as a lack of pregnancy success
166 with wild-type females [Ha et al., 2016].

167 One of the N-DRC structural genes is *TCTE1* (T-Complex-associated-Testis-Expressed 1), known also as
168 *DRC5, FAP155*, *D6S46* in humans (*locus* 6p21.1; MIM:186975) or *Tcte1*, *D17S*, *Tcte-1*, *D17Sil1* in mouse (*locus* 17
169 B3; 17 22.54 cM; MGI:98640). *TCTE1* is evolutionary conserved in most eukaryotic organisms, that contain
170 motility cilia or flagella in their life cycle (Figure 1), and is required for proper flagella functioning. Expression of

171 *TCTE1* is being observed in testis (highest; with expression starting at the stage of spermatid), choroid plexus and
172 Fallopian tube. TCTE1 contains five leucine rich repeats (LRRs). To date, only one report described a role of *Tcte1*
173 gene in infertility, where the sperm cells of *Tcte1-null* mice exhibited asthenozoospermia [Castaneda et al., 2017].
174 However, understanding of the nature of this specific motility type defect in *Tcte1-null* animals has been limited.
175 In our study we aimed to determine the role of *Tcte1* in male infertility using mouse knockout model.
176 We created homo- and heterozygous animals, which were next examined for their reproductive potential,
177 differences in anatomy and histology, and semen parameters. We also performed RNA sequencing (RNAseq) in
178 testis tissue to obtain an answer about the influence of *Tcte1* null mutation on the expression pattern of other
179 gonadal genes. Also, the ATP measurement of spermatozoa has been performed. Additionally, screening of
180 variants in human samples from males with severely decreased sperm count was made, followed by protein
181 prediction modeling of revealed variants. Thus, this study contains novel and the most complete data concerning
182 *TCTE1* role in male infertility, so far.
183

184 **MATERIALS AND METHODS**

185 *Animals*

186 Using CRISPR/Cas9 genome editing technique, mouse heterozygous knockout line of *Tcte1* gene
187 (*Tcte1*$^{+/}$) was created on the basis of C57Bl/6J strain in the Cyagen Biosciences company (USA). The mouse *Tcte1*
188 gene is located on chromosome 17 B3; 17 22.54 cM (GenBank: NM_013688.2; Ensembl:
189 ENSMUSG00000023949). Exon 3 of the *Tcte1* gene was selected as target site (deletion of 1292 bp) (Figure 2A).
190 gRNAs targeting vectors (constructed, sequenced and generated by *in vitro* transcription) were injected into
191 fertilized oocytes (Supplementary file 1). The founders were genotyped and those with positive results were bred
192 to the next generation. Then, in the animal facility of the Institute of Human Genetics PAS (Poznan, Poland), adult
193 *Tcte1*$^{+/-}$ animals were mated to generate homozygous *Tcte1*$^{-/-}$ mice. Wild type *Tcte1*$^{+/+}$ (WT) animals C57Bl/6J
194 were purchased from Charles River company (Germany). Relative expression of *Tcte1* gene was verified using
195 Real-time PCR method (Figure 2B; Supplementary file 2). All mice were housed in pathogen-free animal facility
196 with food and water *ad libitum*, stable temperature of 22°C, and a light:dark light cycle of 12:12. All procedures
197 were in accordance with the guidelines and regulations for animal experimentations and restricted usage of
198 genetically modified organisms (GMO), and were approved by the Local Ethical Committee for Animal
199 Experiments at the Poznan University of Life Sciences (no. 1/2014, 18/2017), and Ministry of Environment (no.

200 70/2017). Mouse models with infertility phenotypes were reviewed in the Mouse Genome Informatics database
201 (Jackson Laboratory; http://www.informatics.jax.org/) and through literature searches (PubMed;
202 https://pubmed.ncbi.nlm.nih.gov/).

203 *Reproductive potential*

204 To check the reproductive potential of KO mice, adult animals (7-8 weeks old) were crossed for delivery
205 of three litters per caged pair, but no longer than for 6 months. Crossing combinations included: (i) 4 pairs:
206 homozygous *Tcte1*$^{-/-}$ male × wild type (WT) female, (ii) 5 pairs: heterozygous *Tcte1*$^{+/-}$ male × heterozygous *Tcte1*$^{+/-}$
207 female, and (iii) 3 pairs: heterozygous *Tcte1*$^{+/-}$ male × wild type (WT) female. Vaginal plug presence was checked
208 every morning to confirm mating incidence. Time period from mating start point to first pedigree appearance
209 was checked. Number of pups was counted on the day after birth. For each crossed pair, the number of litters,
210 pups, and sex ratio were estimated (also according to pups' genotypes) (Supplementary file 3).

211 *Genotyping*

212 Genotyping of the pups delivered was performed via PCR assay, with two sets of primers: (i) to identify
213 wildtype and positive KO (het- and homozygous) animals: Tcte1-F: CGTTTTAAGAATGTATTGAGGGTTGGG, Tcte1-
214 R: CTCCGTAGGCTCCTGCCAATATG; estimated product size: for WT 1915 bp, for KO ~630 bp (deleted ~1300 bp);
215 PCR results analysis: one band with 1915 bp or 0 bp determined WT, while one band with 630 bp evidenced
216 hetero- or homozygotes; (ii) to distinguish between hetero- and homozygotes: Tcte1-WT/He-F:
217 AGCTTGCCACACCCTCAAGGTACTA, Tcte1-R: CTCCGTAGGCTCCTGCCAATATG; estimated product size: 658 bp for
218 heterozygotes and 0 bp for homozygotes; PCR results analysis: one band with 658 bp determined heterozygotes,
219 while no one band (0 bp) indicated homozygotes (Figure 2C). The PCR mixture and reaction conditions are
220 described in Supplementary file 4.

221 *Tissue gonadal preparation/collection*

222 Gross anatomy was performed on testis and epididymis of WT (n=21), *Tcte1*$^{+/-}$ (n=22), and *Tcte1*$^{-/-}$ (n=18)
223 male animals (10 weeks old). Mice were weighted, then euthanized with carbon dioxide (CO_2) overdose
224 (euthanasia Minerve Easy-box; Minerve; France) with stable flow rate per minute. Testes and epididymises were
225 collected, weighted, and measured. For histological evaluation tissues were immersed into 10% formalin
226 solution, neutral buffered (Sigma Aldrich, USA) for 3 males per zygosity. Then, Paraplast-embedded sections were
227 prepared (5 µm thickness), using Microtome Leica 2055. To obtain the histological picture, slides were stained

228 with Masson-Goldner protocol [Romeis et al., 2010]. Thereafter, slides were documented with Leica DM5500
229 light microscope (×1000 magnification, oil immersion).

230 *Mouse semen samples*

231 Mouse spermatozoa were collected from epididymides *post mortem*. Collected epididymides were
232 placed immediately in a 2.0 mL test tube with warm 500 µL of a non-capacitating Whitten's HEPES medium (pH
233 7.2-7.4, 37°C), then cutted into 5-7 fragments, and incubated in 37°C for 15 min. to allow the sperm cells to swim
234 out. Whittens-HEPES medium contained: 100.0 mM NaCl, 4.4 mM KCl, 1.2 mM KH2PO4, 1.2 mM MgSO4, 5.4 mM
235 glucose, 0.8 mM pyruvic acid, 4.8 mM lactic acid (hemi-Ca), HEPES 20 mM [Wertheimer et al., 2013]. Then,
236 spermatozoa were collected and proceeded with seminological analysis (concentration, motility, morphology).
237 Next, semen samples were fixed in a fresh fixative solution (methanol:acetic acid, 3:1 v/v, -20°C; 3×) and stored
238 until further use in -20°C.

239 *Semen analysis*

240 10 µl of sperm suspension was applied on the Makler counting chamber (Sefi medical instrument Ltd.,
241 Israel) to test the sperm concentration and total sperm count. Also, the ratio of progressive (fast and slow), non-
242 progressive (total and circular) and immotile spermatozoa were calculated [WHO, 2020]. For assessment of
243 sperm morphology, the Papanicolaou staining was performed. Briefly, the air-dried smears were fixed in
244 ethanol:diethyl ether (1:1 ratio, vol/vol) solution for 10 min. and left for air-drying. Then, slides were stained by
245 Papanicolau procedure according to WHO guidelines [WHO, 2020], and mounted in DPX Mountant (Sigma-
246 Aldrich; USA; cat. no. 06522). A total of 200 spermatozoa were analyzed using Leica DM5500 light microscope
247 (×1000 magnification, oil immersion). Various morphological forms of spermatozoa were determined including
248 abnormalities of head, midpiece and tail. Also, the length of sperm tail, midpiece and the tail:midpiece ratio were
249 measured to check possible differences between males with various zygosity (6 males/per zygosity); for each
250 male at least 100 spermatozoa were measured with the 'length measurement' option by CellSense Dimension
251 software (Olympus).

252 *Sequencing of RNA (RNAseq)*

253 For RNA extraction testis tissue was collected into in RNAlater buffer (Invitrogen; Waltham, MA, USA)
254 and freezed immediately (-80°C). Samples were processed using the AllPrep DNA/RNA/Protein Mini Kit (Qiagen;
255 Hilden, Germany). Quality and quantity of extracted RNA samples were checked using NanoDrop (Thermo
256 Scientific) and Quantus (Promega), and 1 µg of RNA per sample has been used for sequencing (Macrogen; South

257 Korea). RNA sequencing was performed with Illumina NovaSeq 6000 platform using TruSeq Stranded mRNA LT
258 Sample Prep Kit, with specified conditions of paired-end reads at 100 bp, and throughput 100 M reads per
259 sample. RNA-Seq raw reads were aligned to mouse reference genome mm10 using hisat 2.0.5 with Gencode
260 vM13 transcriptome reference. Reads aligned in the coding regions of the genome were counted using Feature
261 Counts. Then, read counts were normalized using DESeq2 and subjected to differential analysis. The differential
262 analysis included computing of median based fold change, statistical significance using the Students' t-test and
263 false discovery rates (correction for multiple testing) in the R/Bioconductor programming environment. Testis
264 tissue expression was retrieved from GTEx (https://gtexportal.org/home/), BioGPS (http://biogps.org/), and
265 AceView (https://www.ncbi.nlm.nih.gov/IEB/Research/Acembly/). All RNA-seq expression data have been
266 deposited in Gene Expression Omnibus (GEO), accession number GSE207805.

267 *STRING interactions*

268 For analysis of protein-protein interactions, based on changed expression level of corresponding genes
269 identified in the mouse testis RNAseq experiments, the STRING analysis was performed [version 11.0]. STRING
270 database allows to delineate probability of the interactions between evaluated proteins using different evidence
271 channels [Mering *et al.,* 2005; Szklarczyk *et al.,* 2019]. This tool enables the integration of all data available in
272 public resources concerning protein-protein interactions.

273 *Immunofluorescence on sperm – N-DRC visualization*

274 Immunofluorescence *in situ* staining was performed to detect the N-DRC complex proteins: Tcte1 (Drc5),
275 Drc7, Fbxl13 (Drc6), and Eps8l1 (Drc3) in mouse spermatozoa. Mouse spermatozoa were collected and fixed as
276 described above. Specific antibodies were applied: primary antibodies – rabbit anti-human-TCTE1, rabbit anti-
277 mouse-Drc7, anti-mouse-Fbxl13, and anti-mouse-Eps8l1 (all from Biorbyt; Cambridge, UK); secondary antibody
278 – goat anti-rabbit-AF594 (Abcam; cat. no. ab150160; Cambridge, UK). The UniProt IDs and homology of the
279 immunization regions of primary antibodies between human and mouse were described in Supplementary file
280 5. Antibodies were diluted in 0.5% PBST (primary: 1:100, secondary: 1:500). First, slides with fixed sperm smears
281 were washed in a series of washes in 1× PBST, and then incubated in 25 mM DTT/1 M Tris-HCl, pH 9.5, at room
282 temperature for 20 min. Then, washing in 1× PBST, and incubation in 6 N HCl for 30 min. was applied, followed
283 by blocking step with 1% BSA/1× PBST for 30 min. Next, overnight incubation with antibodies was performed at
284 4°C in a humidified container. After washing, the samples with 1× PBST, secondary AF594-conjugated antibody
285 was applied for 1 hr. Next, unconjugated antibodies were washed out (4× in 1× PBST, 5 min each, slight rotation).

286 For the final detection, 20 ul of Fluoroshield with DAPI (Sigma-Aldrich; cat. no. F6057) was added to the samples,
287 and microscopic analysis was performed. Images were acquired using a fluorescence microscope with a proper
288 filter set: Leica DM5500, filters: DAPI/TxR/Triple; objectives: 10× and 63× with oil immersion; DFC 7000T camera;
289 software: LASX.

290 *Sperm ATP measurement*

291 For measurement of ATP in spermatozoa the CellTiter-Glo 2.0 Assay (Promega; USA) was used. This
292 ready-to-use assay allows to determine the quantitation of the ATP amount, indicating the presence of
293 metabolically active cells. The assay is based on the thermostability of luciferase (Ultra-GloTM Recombinant
294 Luciferase), and was performed as described in manufacturers' protocol. Briefly, all laboratory work was done in
295 the stable temperature of 22°C. After collection of mouse spermatozoa (as described above), the amount of
296 approximately 1×10^6 of sperm cells was transferred to black opaque 1.5 mL test tube and proper amount of
297 CellTiter-Glo kit was added (1:1, v:v). Next, 2 min. of orbital mixing of the content was performed to activate cell
298 lysis. Then, after 10 min. of incubation (to stabilize the luminescence), the measurement of luminescent signal
299 was completed using Glomax 20/20 luminometer (Promega; USA). For each sample, three measurements
300 (repeats) were done, each in two time points of 0 and +60 min. Numbers of animals used were: WT (n=7), *Tcte1*$^{+/-}$
301 (n=7), and *Tcte1*$^{-/-}$ (n=6). Mean luminescence values obtained (represented as RLU – relative luminescence unit)
302 were compared between tested mice groups.

303 *Immunofluorescence on testis – apoptosis evaluation*

304 Immunofluorescence *in situ* staining was performed to check the level of apoptosis via caspase 3
305 visualization on mouse testis samples from all the three zygosities. Caspases play important role in the induction,
306 transduction, and amplification of intracellular apoptotic signals, and thus, caspase-3 can be used as one of the
307 apoptotic indicators [Lej et al, 2022]. Mouse testes were collected and fixed as described above. Specific
308 antibodies were applied: primary antibody – rabbit anti-human-Casp3, (Biorbyt; Cambridge, UK), diluted 1:100
309 in 0.5% PBST; secondary antibody – goat anti-rabbit-AF594 (Abcam; Cambridge, UK), diluted 1:500 in 0.5% PBST.
310 First, slides with paraffine fixed testis cross sections were deparaffinized in 3 changes of xylene (10 mins. each),
311 and incubated in a series of ethanol: 100%, 96%, and 70%, twice for 5 mins. in each solution. Next, after rinsing
312 in distilled water, tissue sections were incubated sequentially in: a freshly prepared 2% $NaBH_4$/1× PBS, and in
313 0.1M glycine (30 min., room temp. each). Heat-induced epitope retrieval was performed by immersing the slides
314 in a 0.01M sodium citrate/0.05% Tween 20, pH 6.0 for 30 min., followed by cooling down in a room temp. for

315 next 20 min. Blocking step was done in an aliquot of freshly prepared 1% BSA/1× PBST, at 37 °C for 1 h. Then,
316 tissue sections were incubated with primary antibody in a humidified container overnight at 4°C. Secondary
317 antibody was applied for 1 hr, followed by the washing out of the unconjugated antibody (4× in 1× PBST, 5 min
318 each, slight rotation). For the final detection, 20 μl of Fluoroshield with DAPI (Sigma-Aldrich; cat. no. F6057) was
319 added. Images were captured using a fluorescence Leica DM5500 microscope with a proper filter set:
320 DAPI/SpO/Triple; objectives: 10× and 63× with oil immersion; DFC 7000T camera, LASX software. The analysis
321 was performed for three independent males per zygosity, 2 cross-sections each time, 15-20 tubules per tissue
322 section.

323 *Sequencing of the human samples*

324 A pilot genomic sequencing study of samples from human infertile males was also applied. DNA from
325 whole blood samples (collected into sterile single test tubes with EDTA) was extracted using standard protocols
326 of MagCore HF16 Automated Nucleic Acid Extractor (RBC Biosciences, Taiwan), or Gentra Puregene kit (Qiagen,
327 USA). Total number of sequenced patients was n=248, including: 137 with non-obstructive azoospermia (lack of
328 spermatozoa in ejaculate) or cryptozoospermia (spermatozoa detectable in ejaculate after centrifugation),
329 followed by 111 samples with spectrum of seminal abnormalities in concentration, and/or motility, and/or
330 morphology. Among those samples, 47 revealed decreased motility (asthenozoospermia). Semen evaluation was
331 done according to WHO guidelines [WHO, 2020], followed by AUA and ASRM guidelines for infertile male
332 diagnosis [Schleger et al., 2021]. All men revealed normal hormonal levels, had no chromosomal abnormalities
333 and a lack of AZF microdeletions. For whole exome samples (n=76 from Pittsburgh), sequencing libraries were
334 constructed using the Agilent technologies (Santa Clara, USA), including: SureSelect XT All Exon V4 + UTRs capture
335 kit and SureSelect XT Target Enrichment System. Libraries were sequenced with average read coverage of 62-
336 100x (~6Gb per sample), using 100 bp paired-end sequencing with TruSeq PE Cluster Kit v3 cBot HS and 4 × 50
337 TruSeq SBS V3 HS sequencing kit (Illumina, San Diego, USA) on the HiSeq2000 (Illumina, San Diego, CA). Whole
338 genome sequencing (n=42, Poznan) was performed using Illumina HiSeqX with the coverage of at least 30x (100-
339 120 Gb per sample). Sanger sequencing for all exomes of *TCTE1* gene (n=130, Poznan) was performed using
340 LightRun96 system of Eurofins Genomics (Eurofins Genomics AT GmbH, Vienna, Austria). Samples were prepared
341 with QIAquick Gel Extraction (cat. no. 28704) or PCR Purification (cat. no. 28104) kits (Qiagen, USA), and analyzed
342 with CLC Main Workbench 8 software (Qiagen, USA).

343

344 *Filtering of whole genome sequencing results*

345 The quality of raw NGS data was evaluated using the FastQC and MultiQC packages. Reads were aligned to the
346 reference human genome GRCh37 using bwa-mem aligner included in the Speedseq package [Chiang et al.,
347 2015]. For calling of single nucleotide variants (SNVs) and small indels the freeBayes v0.9.21 (speedseq-var) was
348 implemented, following previously described pipeline [Supernat *et al.,* 2018]. Variant disease association and
349 missense mutation prediction effects were determined using: dbSNP (https://www.ncbi.nlm.nih.gov/snp/),
350 OMIM (https://www.ncbi.nlm.nih.gov/omim/), ClinVar (https://www.ncbi.nlm.nih.gov/clinvar/),
351 MutationTaster (http://www.mutationtaster.org/), SIFT (https://sift.bii.a-star.edu.sg/), Polyphen
352 (http://genetics.bwh.harvard.edu/pph2/), CADD (https://cadd.gs.washington.edu/snv), MetaDome
353 (https://stuart.radboudumc.nl/metadome/), REVEL (rare exome variant ensemble learner) [Ioannidis et al.,
354 2016], Ensembl Variant Effect Predictor [Mclaren et al., 2016], and Human Gene Mutation Database (HGMD;
355 Qiagen, Redwood City, CA). SNV pathogenicity was assessed on the basis of American College of Medical Genetics
356 and Genomics (ACMG) guidelines [Richards et al., 2015]. PhyloP (Cold Spring Harbor Laboratory) and Clustal
357 Omega were used for determination of conservation (https://www.ebi.ac.uk/Tools/msa/clustalo/). All NGS
358 variants were confirmed via the Integrative Genomics Viewer (Broad Institute). Variant frequencies have been
359 obtained from the gnomAD database (frequencies from more than 125k exomes and 15k genomes,
360 http://gnomad.broadinstitute.org; v2.1.1), and were filtered in search of rare variants (with minor allele
361 frequency (MAF) <1%).

362 *Protein prediction*

363 The amino acid sequence of TCTE1 was input into Phyre2 [Kelley et al., 2015] for both intensive and fast
364 mode homology modeling, I-TASSER [Roy *et al.,* 2010; Yang *et al., 2*015, Yang and Zhang 2015], and AlphaFold
365 [Jumper *et al.,* 2021; Varadi *et al.,* 2022] which utilize sequence alignment-based algorithms for generating
366 predicted secondary and tertiary structures; AlphaFold additionally uses machine learning to integrate biological
367 principles of protein folding with the alignment-based algorithms. Confidence scores were obtained from these
368 programs; AlphaFold additionally generates predicted aligned error plots for assessing the quality of the model's
369 long-range interactions. Models were inspected manually and aligned using the secondary structure matching
370 (SSM) [Krissinel and Henrick, 2004] tool in COOT [Emsley *et al.,* 2010] to minimize user input bias. Docking of the
371 structures into electron tomography data was performed manually in COOT [Emsley *et al.,* 2010]. No refinement
372 was performed to minimize bias. All structure model figures and mutations without post refinement, were

373 generated using Pymol (Schrödinger). I-TASSER was used also for prediction of the exon 3 structure deleted in
374 our mouse KO model (Supplementary file 6).

375 *Statistical analysis*

376 Statistical analyses included the following: normality test (D'Agostino and Pearson or Kolmogorov-
377 Smirnoff), unpaired two-tailed t-test with Welch's correction, one-way ANOVA test and Fisher's exact, and two-
378 tailed Pearson correlation. All tests were performed with a significance level of α=0.05 using GraphPad Prism
379 (v.7.0e) software.

380

381 **RESULTS**

382 *Reproductive potential of KO mice*

383 Reproductive potential results were shown in Figure 3 and Supplementary file 3. Only pairs with
384 homozygous *Tcte1*$^{-/-}$ males revealed no progeny (*Tcte1*$^{-/-}$ male x WT female). Other combinations (*Tcte1*$^{+/-}$ male
385 × *Tcte1*$^{+/-}$ female; *Tcte1*$^{+/-}$ male × WT female) showed similar results, when considering: number of litters, pups,
386 and sex ratio. Mean time of caging to delivery of the 1st pedigree was longer in *Tcte1*$^{+/-}$ male × *Tcte1*$^{+/-}$ female
387 combination by 25.45% (statistically not significant). When considering genotypes of the pups, statistically
388 significant differences ($p<0.05$) were observed in the number of *Tcte1*$^{-/-}$ male and female pups delivered – no
389 homozygous animals were obtained from combination of *Tcte1*$^{+/-}$ male × WT female, while in mating of *Tcte1*$^{+/-}$
390 male × *Tcte1*$^{+/-}$ female, homozygous males (33.25% of all pups) and females (24.67%) were received.

391 *Histopathology and seminal parameters*

392 Histopathological evaluation of testicular and epididymal sections revealed no differences between WT,
393 *Tcte1*$^{+/-}$, and *Tcte1*$^{-/-}$ males (Figure 4A). No odds were found for body mass of the animals and the length of the
394 epididymis (Figure 4B). In the *Tcte1*$^{-/-}$ males testis weight was decreased by approximately 41% ($p<0.0001$)
395 followed by the ~22% decline of its size ($p<0.0001$), while in *Tcte1*$^{+/-}$ males only testis weight was slightly
396 decreased (approx. 7%; $p<0.05$) when compared to control animals.

397 When considering seminal parameters, both: in *Tcte1*$^{-/-}$ as well as in *Tcte1*$^{+/-}$ males the sperm
398 concentration was importantly decreased (3.27, and 2.47-fold, respectively), when collating to control results
399 ($p<0.0001$; Figure 4C). Additionally, in *Tcte1*$^{-/-}$ males the frequency of progressively motile spermatozoa was
400 residual, with progressive type of motility in only 0.22% of spermatozoa (decreased ~150-fold vs. control 33.52%,
401 ($p<0.0001$)), followed by 4.89% of slow progressive spermatozoa (decreased ~3-fold vs. control 15.50%)

402 (p<0.0001). Interestingly, ~2.4-fold increase in circular type of motility (around own axis and non-progressive)
403 was observed for *Tcte1*$^{-/-}$ males when compared to WT and *Tcte1*$^{+/-}$ animals (p<0.01) (Supplementary file 7;
404 Supplementary file 8; Supplementary file 9). The frequency of immotile spermatozoa also increased in *Tcte1*$^{-/-}$
405 males (2-fold to control; p<0.0001). The frequency of morphologically normal spermatozoa in *Tcte1*$^{-/-}$ animals
406 was significantly decreased (2-fold to control; p<0.0001; Figure 4C, D, E; Supplementary file 10). The majority of
407 morphological defects was observed for sperm head, mostly of decapitated spermatozoa in *Tcte1*$^{-/-}$ animals –
408 52.55% vs. 19.16% for *Tcte1*$^{+/-}$ and 23.33% for WT, and amorphous head shape with decreased frequency in
409 *Tcte1*$^{-/-}$ (26.11%) and *Tcte1*$^{+/-}$ (33.72%) males vs. WT animals (48.88%) (Supplementary file 10). Midpiece defects
410 were found in *Tcte1*$^{+/-}$ (9.71%) and WT (8.20%) animals, while *Tcte1*$^{-/-}$ mice revealed only low frequency (0.38%)
411 of such defects. On the other hand, an increased frequency (~5-fold) of coiled tail was observed for *Tcte1*$^{+/-}$
412 animals when compared to other mice zygosity (p<0.01) (Supplementary file 10). Summarizing, seminological
413 changes in mice with *Tcte1* mutation resulted in oligoasthenoteratozoospermia in homozygous *Tcte1*$^{-/-}$ or
414 oligozoospermia in heterozygous *Tcte1*$^{+/-}$ animals.

415 Increased mean length of tail and tail:midpiece ratio in *Tcte1*$^{-/-}$ animals (139.30 ± 7.71 um; 5.16,
416 respectively) was measured when comparing to WT (122.00 ± 6.375 um; 4.51; p<0.002) and *Tcte1*$^{+/-}$ (123.50 ±
417 1.89; 4.83; p<0.008) (Figure 4F). Also, in the *Tcte1*$^{+/-}$ the midpiece length differed from *Tcte1*$^{-/-}$ animals
418 (p=0.0334), followed by tail:midpiece ratio differences when compared to WT (p=0.0435).

419 *Sequencing of RNA (RNAseq) and STRING pathway analysis*

420 RNA sequencing analysis of gene expression in testes of KO mice revealed statistically significant
421 changes (p<0.05) in 21 genes, including 5 genes both for *Tcte1*$^{-/-}$ vs. *Tcte1*$^{+/-}$ and WT, 8 genes only for *Tcte1*$^{-/-}$ vs.
422 WT, 7 genes only for *Tcte1*$^{-/-}$ vs. *Tcte1*$^{+/-}$, and 1 gene both for *Tcte1*$^{+/-}$ vs. *Tcte1*$^{-/-}$ and WT (Figure 5). In *Tcte1*$^{-/-}$
423 animals vs. both: *Tcte1*$^{+/-}$ and WT, the expression level of 4 genes from kallikrein subfamily was decreased 2-8-
424 fold, including genes involved in semen liquefaction and degradation of extracellular matrix proteins in the
425 interstitial area surrounding Leydig cells of the adult mouse testes (*Klk1b27*, *Klk1b21*, *Klk1b24*), or neuronal
426 activity (*Klk1b22*) (Figure 5; Supplementary file 11) [Michaelis *et al.,* 2017; Marques *et al.,* 2016; Du Plessis *et al.,*
427 2013; Fink *et al.,* 2007]. 2-fold decrease of expression of genes related to mitochondrial cytochrome oxidase
428 subunits and asthenozoospermia was documented (*mt-Co2*, *mt-Co3*) (Figure 5) [Heidari *et al.,* 2016; Mostafa *et*
429 *al.,* 2016; Baklouti-Gargouri *et al.,* 2013]. In a scheme: *Tcte1*$^{-/-}$ vs. WT, 8 genes revealed changes in expression
430 level, including 4.7-fold rise for *Fetub* gene, which is known as required for egg fertilization (via specific inhibitor

activity of the *zona pellucida* (ZP) ovastacin, the cysteine protease responsible for ZP2 cleveage) [Binsila *et al.,* 2021; Karmilin *et al.,* 2019], and plays also a role of a secreted factor during reprogramming [Bansho *et al.,* 2017].

Two-fold rise for *Igf2* gene (strongly linked to spermatogenesis, sex determination, testis development, infertility and prostate cancer; [Matsuzaki et al., 2020; Cannarella et al., 2020; Neirijnck et al., 2019; Damaschke et al., 2017]) has been also noticed. Igf2 and Klk proteins are enclosed in a common network consisted of proteins directly linked to fertility (Figure 6; Supplementary file 11; Supplementary file 12). One of them is Ambp, a fusion protein, which proteolysis generates bikunin – a protein which deficiency results in infertility, due to the diminished formation of the stable cumulus-oocyte complex required for maturation and ovulation [Sato and Kan,2001; Naz and Rajesh, 2005]. Bikunin is one of the elements of ITIH domains (Inter-α-Trypsin Inhibitor Heavy-chain), responsible for hyaluronian metabolism [Hull *et al.,* 2012; Salustri *et al.,* 2019]. ITIH is also linked to Plg, which has the protease activity and activates metalloproteins, such as: Mmp8 and Mmp9, also included in the network. Mmp8 is engaged in degradation/stabilization of occluding and blood-testis barrier [Chen *et al.,* 2018], while Mmp9 (with Igf1 and Igf2), is important for normal placentation [Ghosh *et al.,* 2011]. Igf1 and Igf2, are related to Igfbp3, which interacts with humanin expressed in Leydig cells. Humanin together with IGFBP3 and Bax prevents the activation of germ cell apoptosis [Jia et al., 2015; Lue et al., 2021]. What is important, expression of *IGFBP3* is regulated by *HOXD10* gene [Xue *et al.,* 2013; Pan *et al.*, 2021], of which expression has been found with 2.9-fold rise in our study. *Hoxd10* is involved in prostate cancer processing, cell differentiantion and morphogenesis [Jonkers *et al.,* 2020; Mo *et al.,* 2017; Zhang *et al.,* 2019].

Another gene with 2.2-fold expression rise is *Slc45a3,* a well-known marker of prostate cancer progression, when a loss of the protein determined poorer prognosis for cancer patients [Hernández-Llodrà *et al.* 2017; Pin *et al.,* 2017; Perner *et al.,* 2013]. An overexpression of another gene identified in our study (12-fold rise for *Usp39* gene) is linked with promotion of prostate or ovarian tumorigenesis. *Usp39* is also involved in pre-mRNA splicing, cytokinesis and spindle checkpoint working, and is crucial for apoptosis [Huang *et al.,* 2016; Yuan *et al.,* 2021; Zhao *et al.,* 2016].

Also, 2.2-2.5-fold rise for ncRNA genes (*Gm26848*, *Gm45648*; no data concerning their role) and 2-fold reduction for one pseudogene (*Gm28661*; also no data) were found (Figure 5). Following the latest data (November 2021) from Gene NCBI database, the Gm45648 has been annotated as one with the testis-restricted expression in mouse but no function has been suggested. The second ncRNA *Gm26848* found is suggested as protein coding organic cation transporter-like protein across membranes in *Drosophila sechellia*. There were also

460 two other genes with expression change (3.6-fold decrease – pseudogene *Gm44126*, and 2.5-fold increase –
461 *4933430L12Rik* probably involved in antisense transcription). 'Gene' database data showed that the *Gm44126*
462 in mice is rather a protein coding gene with the function of UDP-glucuronic acid decarboxylase, and contains two
463 domains involved in NAD(P)H processing. Thus, it can be suggested that this gene is as a novel candidate involved
464 in mitochondrial respiratory chain. Our data with 3.6-fold expression decrease of this gene seem to fit into
465 observed diminished functioning of mitochondrial machinery in *Tcte1*$^{-/-}$ mice.

466 Another three genes manifested 2-fold decrease of their testis expression when comparing *Tcte1*$^{-/-}$ vs.
467 *Tcte1*$^{+/-}$ (but not to WT): *Aqp2* (aquaporin-2 involved in osmotic transportation of the water), with well-known
468 role in spermatogenesis, female endometrium cycle and urinary incontinenece; [Klein *et al.,* 2013; Ramli *et al.,*
469 2019], *Mt3* (metallothionein-3, committed in homeostasis and detoxification of toxic metals, also in testis)
470 important in apoptosis regulation of Bax and Caspase pathways [Gao *et al.,* 2021; Honda *et al.,* 2010]), and
471 *Rps27rt* (ribosomal protein) (Figure 5; Supplementary file 11). It was also found that Rps27rt may interact
472 indirectly with Usp39 and mitochondrial respiratory complex linking the mitochondrial energy processing with
473 apoptosis (Supplementary file 11). Last gene – *Ube2l6*, was found to have 2-fold increased expression level in
474 testis in *Tcte1*$^{+/-}$ animals vs. *Tcte1*$^{-/-}$ and WT. Its role has been established as ubiquitin enzyme engaged in: stress
475 damage response, cell cycle progression, embryo development, immune response, and factors linked to ATP
476 machinery (Figure 5) [Huang *et al.,* 2016; Yuan *et al.,* 2021; Zhao *et al.,* 2016; Sandy *et al.,* 2020; Cai *et al.,* 2021].
477 Increased expression of *Ube2l6* was linked to degradation/suppression of cancer cells and affected downstream
478 apoptotic factors (i.e., Caspase 3, Caspase 9, Bcl-2, Bax) [Li *et al.,* 2018].

479 *Immunofluorescence on sperm*

480 An example of immunofluorescence *in situ* staining on mouse spermatozoa used to detect the N-DRC
481 proteins has been presented in Figure 7. WT mouse spermatozoa showed Tcte1 protein presence in the sperm
482 head nucleus, midpiece, and a part of the tail (Figure 7A). Immunofluorescent signal of Tcte1 in *Tcte1*$^{+/-}$ mice was
483 similar to WT animals, while in *Tcte1*$^{-/-}$ was localized only in the nucleus (Figure 7A). It seems to confirm that in
484 *Tcte1*$^{-/-}$ males the protein has not been produced properly, revealing only residual amounts in sperm head
485 nucleus, and not transported to sperm flagella. The other N-DRC components (Drc7, Fbxl13 and Eps8l1) were
486 localized in the sperm nucleus and among the whole sperm tail (Fbxl13, Eps8l1) or only within its fragment (Drc7),
487 with exception of the midpiece (Figure 7B). Results obtained seem to suggest co-localization of evaluated N-DRC
488 proteins in various combinations, not common among the midpiece and the terminal part of the sperm tail.

489 *Sperm ATP level*

490 Measurements performed in two time points (0 and +60 min.) revealed that in *Tcte1*$^{-/-}$ samples the
491 luminescence level was approximately 2.4-fold lower when compared to WT and *Tcte1*$^{+/-}$ mice ($p<0.0001$) (Figure
492 8; Supplementary file 13). There were no differences between WT and *Tcte1*$^{+/-}$ males. Additionally, the decrease
493 of the luminescent signal after 60 min. was similar in all three groups studied – approximately by 35% (WT:
494 35.27%, *Tcte1*$^{+/-}$: 33.88%, *Tcte1*$^{-/-}$ 37.76%).

495 *Apoptosis in testicular tissue*

496 Evaluation of the immunofluorescent staining results revealed Casp3-positive signals (indicating
497 apoptosis) in spermatogonia only, in all three mouse genotypes (Figure 9). In each zygosity the numbers of
498 tubules and positively stained spermatogonia (intensity of the signal) were similar suggesting equal levels of
499 apoptosis.

500 *Sequencing – human male samples*

501 Potentially associated/important 6 heterozygous SNVs for *TCTE1* gene has been found in 15 out of 248
502 (6.05%) infertile males with drastically decreased semen parameters, ranging from azoospermia to severe
503 oligoasthenozoospermia (Table 1). 3 variants were identified with ultrarare allele frequency (MAF ≤0.0005 in the
504 general population; gnomAD) in three males with NOA: c.862C>T (p.Arg288Ter) predicted as stop-gained
505 mutation leading to non-mediated decay, and thus to protein loss of function with high probability; c.185G>A
506 (p.Arg62His), or c.1048G>A, (p.Gly350Ser), defined as missense ones and probably damaging. Next two SNVs
507 were found as the rare missense ones with MAF <0.005: c.397C>T (p.Arg133Cys) (one NOA case) and c.470A>C
508 (p.Glu157Ala) (four NOA cases), and were defined as probably damaging. The last 1 SNVs (1 NOA, 1 crypto-, and
509 5 with severe oligoasthenozoospermia) was not found in databases, and thus specified as the novel one
510 (c.374T>G; p.Ile125Arg) with missense prediction (Table 1; Supplementary file 14).

511 *Protein prediction*

512 To understand the molecular implications of identified mutations on the structure and function of
513 TCTE1, we performed homology modeling experiments using the Phyre2, I-TASSER, and AlphaFold tools [Kelley
514 *et al.,* 2015; Roy *et al.,* 2010; Yang *et al.,* 2015; Yang and Zhang 2015; Tunyasuvunakool *et al.*, 2021]. TCTE1 is
515 predicted to contain at least five tandem leucine-rich repeats (LRR) in its C-terminus [UniProt 2019], while no
516 known three-dimensional protein folds have been assigned to its N-terminus. All homology searches yielded a
517 polypeptide with tandem leucine-rich repeats with nearly 100% confidence (Figure 10A; Supplementary file 15).

518 Modeling the N-terminal region of TCTE1 was more difficult; although both Phyre2 and I-TASSER confidently
519 predicted a largely α-helical secondary structure for the N-terminal half of TCTE1 (Figure 10A; Supplementary
520 file 15), neither tertiary structure was predicted with high confidence; indeed, comparison of the two
521 demonstrates vastly different folds for the N-terminus from the programs. However, the confidence of the
522 AlphaFold-generated model was high for the region just N-terminal to the LRR. Further, based on the predicted
523 aligned error plot for calculated for its models, the confidence of the predicted structure of residues 100-200
524 was high relative to the position of residues 220-480, providing support for the modeled through-space three-
525 dimensional interactions. That said, we interpreted these models very conservatively.

526 We attempted to hypothesize how mutations of interest could affect the tandem LRRs and putative
527 secondary structure of the N-terminus of the protein. Residue R64 resides in a predicted unstructured region
528 and as such most likely is solvent exposed in the tertiary structure (Figure 10A, B). Mutation of this residue from
529 arginine to histidine could therefore affect the surface potential of this disordered region, making the it less
530 positively charged. Indeed, this mutation would be expected to impact the interactions that the N-terminus of
531 TCTE1 can have with other molecules, including other members of the N-DRC. The interaction of microtubule-
532 associated proteins, including the N-DRC, with binding partners is known to be largely charge-based [Kubo *et al.,*
533 2017; Drechsler *et al.,* 2019].

534 Three mutations of interest occur in the globular region just N-terminal to the LRR. The AlphaFold model
535 clearly shows how mutation I125R would affect the structure of this region Figure 10a, c). Residue isoleucine 125
536 is predicted to be nestled within the hydrophobic core including L97 L109, L112, F91, W131, L197, Y130, and the
537 methyl group of the T121 sidechain. A substitution of positively charged arginine for isoleucine in this position
538 would not be accommodated in this hydrophobic region, likely resulting in local unfolding that could potentially
539 propagate beyond the pocket. Likewise, residue R133 supports the structure of this putative globular domain by
540 forming hydrogen bonds with the backbone of residues 109, 110, and/or 112, thereby possibly contributing to
541 the overall organization of this domain and its positioning relative to the LRR (Figure 10d). Mutation of this
542 residue to a cysteine would remove the hydrogen bonding groups supporting these interactions, likely leading
543 to a local unfolding that could possibly propagate farther. Interestingly, residue E157 is predicted to interact with
544 residues in the LRR, likely stabilizing positively charged residues around it, including several from the linker
545 leading up to the first β-strand of the LRR (Figure 10B, E). Mutation of this residue to an alanine would lead to a

546 tertiary destabilization, most likely affecting the overall structure of the N-terminal region of the LRR and the
547 globular region just N-terminal to it.

548 Two mutations of interest affect the LRR helices. Mutation R288* results in premature truncation,
549 eliminating most of the LRR region from the final protein product, although it is predicted that this premature
550 termination codon would lead to nonsense mediated decay. Mutation G350S would be expected to result in the
551 destabilization of inter-repeat interactions (Figure 10F), possibly even unfolding the protein from that position
552 on; the lack of a side chain in glycine allows for the close approach of these tandem structural elements, whereas
553 the addition of the serine side chain would abrogate the tight packing of residues, regardless of which rotamer
554 it adopts. This could result in a restructuring its C-terminus and/or deforming the surface of the module,
555 therefore affecting its interactions with its binding partners.

556 Since the N-DRC is conserved from single-celled eukaryotes to mammals, we took advantage of
557 published cryo-electron tomography studies examining the N-DRC from model organism *Chlamydomonas* (1).
558 This study was of great interest since it explicitly located the position of the C-terminus of DRC5 with a nanogold
559 particle; importantly, it was consistent with earlier cryo-ET experiments positioning the N-DRC (2). While the
560 resolution of this structure is only 40Å, it was still useful for placing the modeled TCTE1 structure in the context
561 of the entire N-DRC (Supplementary file 15B). Manual docking of the AlphaFold predicted TCTE1 structure is
562 consistent with the cryo-EM tomography data [Gui *et al.,* 2019; Heuser *et al.,* 2009].

563

564 **DISCUSSION**

565 In this study we have investigated the role of *Tcte1* in male infertility using mouse knockout model.
566 Using homo- and heterozygous animals, their reproductive potential has been examined, noting no progeny by
567 homozygous males. While there were no differences in histology of the testes, the size of the gonads varied
568 between the zygosity of animals, followed by two semen phenotypes revealed within the sperm quality
569 evaluation. RNAseq analysis of the mutant testicular tissue demonstrated the influence of *Tcte1* mutations on
570 the expression pattern of genes related to mitochondrial cytochrome oxidase activity, apoptosis and
571 spermatogenesis. The ATP level estimate of spermatozoa showed its decrease in homozygous males.
572 Additionally, protein prediction modeling of identified variants in human samples revealed changes in the protein
573 surface charge potential, leading to disruption in helix flexibility or dynamics, and thus, suggesting the disrupted
574 TCTE1 interaction with its binding partners within the axoneme. The major findings concerning observed

575 abnormal sperm tail beating in KO *Tcte1* mice were summarized in Figure 11. We have also identified and
576 discussed novel functions of genes with testicular expression significantly disturbed in the *Tcte1* knockout.
577 Therefore, this study contains novel and the most complete data concerning *TCTE1* role in male infertility, so far.

578 *Phenotypes of homozygotes and heterozygotes*

579 There was only one published study so far, concerning knockout mouse model of *Tcte1* [Castaneda *et*
580 *al.,* 2017], with Authors the infertile homozygous males due to asthenozoospermia derived from limited and
581 circular flagellar beating, and fertile heterozygotes. The study did not find any differences between homozygous
582 and WT males in the testicular histology, followed by similar testis weight, sperm concentration and sperm
583 morphology [Castaneda *et al.,* 2017]. We also have not found any differences in the testicular and epididymal
584 tissues histology. However, the weight of the testes was decreased significantly (~41% in *Tcte1*$^{-/-}$, 7% in *Tcte1*$^{+/-}$
585), followed also by testis size reduction in *Tcte1*$^{-/-}$ animals (by 22%) (Figure 4B). When comparing semen
586 parameters (Figure 4C-E), we have found enormous decline in sperm concentration in both: *Tcte1*$^{-/-}$ (3.3-fold) or
587 *Tcte1*$^{+/-}$ (2.5-fold) males, and double increase in abnormal sperm morphology in *Tcte1*$^{-/-}$ animals. Similarly, to
588 Castaneda *et al.* [2017], we have documented the impaired sperm motility representing circular mode of the
589 sperm tail beating. Also, the increased ratio of immotile spermatozoa in homozygous males was documented in
590 our study. We can suggest that these discrepancies may result from various number of animals used for
591 evaluation: 3 males in study of Castaneda *et al.,* [2017] vs. at least 18 per each zygosity in our study, when
592 comparing semen parameters and tissue characteristics (except of sperm morphology evaluation with at least 5
593 animals used). Probably, also the differences in knockout construction used could be causative for observed
594 variances: reporter-tagged insertion with conditional potential vs. the exon 3 deletion. Thus, we have observed
595 two various phenotypes dependent on the zygosity of the animals: homozygous males manifested
596 oligoasthenoteratozoospermia (OAT) and were infertile, while heterozygous males demonstrated
597 oligozoospermia (O) and remained fertile. Data collected in International Mouse Phenotypic Consortium (IMPC;
598 a repository of all available mouse phenotypes created, followed with the possible linkage to human disease
599 defects; https://www.mousephenotype.org), concern only one *Tcte1* mouse study [Castaneda *et al.,* 2017], while
600 we reveal an unmatched phenotypes of decreased sperm count.

601 We suggest that similar effect – decreased sperm count linked to *TCTE1* mutations, could be observed
602 in humans. Our pilot mutation screening of 248 human infertile males with severely decreased sperm count
603 (from oligo-, via crypto-, to azoospermia) revealed 6 heterogeneous SNVs (1 novel, 3 ultrarare, and 2 rare; all

predicted as disease causing) with the total frequency of 6.05% (Table 1). We propose that molecular epidemiology studies of infertile patients should reveal the existence of homozygous or a compound heterozygous *TCTE1* variants with clear direct downgrading effect on spermatogenesis. However, we claim that also heterozygous variants can be causative, similarly to *SPINK2* which deficiency has been documented as responsible for oligoasthenozoospermia in heterozygous mice vs. azoospermia in homozygous animals, followed by the azoospermia in human homozygous brothers vs. their heterozygous father with oligozoospermia [Kherraf *et al.,* 2017]. It can be explained by the probable haploinsufficiency occurrence, when the single copy of the WT allele in heterozygous combination of which a variant allele is insufficient to produce the WT phenotype. Our observations, followed by the *SPINK2* data and data related to infertility (i.e.: P1/P2 protamines, *Pde8b*, *Trim28*, *Tcfl5*), and to the other diseases (i.e.: *PIKFYVE* in cataract, *NFIA*, *SCN1A* in neurological or epilepsy disturbances, *KLF1* in hemoglobin persistenece, *NR5A2* in pancreatic cancer), seem to confirm that the severity of the phenotype depends on the gene expression level [Jodar and Oliva, 2014; Mei *et al.,* 2022; Ogura *et al.,* 2022; Heshusius *et al.,* 2022; Valassina *et al.,* 2022; Sandhu *et al.,* 2021; Leal *et al.,* 2021; Tan *et al.,* 2020; Xu *et al.,* 2022]. We have documented variable phenotypes for a novel *TCTE1* variant c.374T>G (p.Ile125Arg) that has been documented in seven males, including: azoospermia, crypto-, and severe oligoasthenozoospermics. Thus, it seems to suggest the reasonable candidacy of haploinsufficiency as the mechanism responsible for observed phenotypic spectra also in case of the *TCTE1* gene.

Kallikreins, Aquaporin 2

Our pathway analysis revealed a network including two genes with changed expression level in testis: *Igf2* (2-fold increased) and *Klk1b22* (8-fold decreased), supported by an interesting set of proteins linked to apoptosis and cellular processing (Figure 5; Figure 6; Supplementary file 11; Supplementary file 12). We can suggest that observed *Igf2* overexpression in our study can be one of the associated factors leading to decreased sperm count and testis parameters in evaluated KO mice model because of its known relation to spermatogenesis and testis development [Matsuzaki *et al.,* 2020; Cannarella *et al.,* 2020; Neirijnck *et al.,* 2019; Damaschke *et al.,* 2017]. Documented reductions can be supported by the observed constrained expression of *Klk1b22* – kallikrein mostly known from its neuronal activity; however, it cannot be excluded that we have revealed additional role of this protein, similar to the other members of the kallikrein family – role in semen liquefaction and degradation of extracellular matrix proteins in the interstitial area surrounding Leydig cells of the adult mouse testes (*Klk1b27*, *Klk1b21*, *Klk1b24*) [Michaelis et al. 2017; Marques *et al.,* 2016, Du Plessis *et al.,* 2013; Fink *et al.,* 2007]. Notably,

633 *Klk1b22* expression is significantly enriched in testis. While expression of all four kallikreins was decreased 2.5-
634 8-fold in our *Tcte1* KO model, indicating their participation in the reduction of sperm parameters measured
635 (Fig.5).

636 We have also documented 2-fold decrease of expression of *Aqp2* (Aquaporin 2), involved in fluid
637 resorption and water movement within the duct system, with known role in spermatogenesis [Klein *et al.,* 2013;
638 Ramli *et al.,* 2019]. It was documented that in stallions Aqp2 is being expressed in Leydig cells, round and
639 elongated spermatids [Klein *et al.,* 2013]. Also, this protein works within a network of molecules that are linked
640 to cell membrane trafficking (i.e., Rab11a, Myo5b), followed by activity of protein kinases (Prkacb, Prkaca) that
641 are known as regulators of cell proliferation, chromatin condensation/decondensation, and nuclear envelope
642 disassembly/reassembly, and all is supported by the ATP metabolism (Hspa8) [Supplementary file 11] [Markou
643 *et al.,* 2022; Wagner *et al.,* 2022]. Considering this evidence, we suggest Aqp2 play an important role in reduction
644 of the spermatids volume during spermatogenesis and in proper sperm morphology assessement and observed
645 morphological differences between *Tcte1* mice zygosities in our study.

646 *Disruptions in sperm cell structure*

647 TCTE1 protein contains five leucine rich repeats (LRRs) that are known to be directly involved in
648 receptor-mediated signaling on the structural basis for interaction between proteins [Ng *et al.,* 2011; Kobe and
649 Kajava 2001]. It was documented that variants in genes encoding LRRs are commonly implicated in the
650 pathogenesis of more than 60 human diseases [Ng *et al.,* 2011; Matsushima *et al.,* 2019]. LRR mutations mostly
651 occur within regions that are protective for the hydrophobic core of the LRR domains. Thus, mutations in LRRs
652 may affect the charge of the surface potential, leading to conformational changes of the protein or induction of
653 protein cumulation. Our prediction model of potential changes in TCTE1 protein resulting from mutations found
654 in human samples seems to point out the prospective impact into the interactions of the TCTE1 with other
655 molecules (binding partners) known to be largely charge-base, including N-DRC elements or microtubule-
656 associated proteins [Kubo et al., 2017; Drechsler et al., 2019]. In the case of TCTE1 protein observed amino acid
657 substitutions promote the abnormal aggregation of TCTE1 protein, and decrease its structural stability, then
658 probably leading to the observed disturbances. Beating motion of flagella is maintained by electrostatic cross-
659 bridge between negatively charged tubulins and positively charged N-DRC [Kubo *et al.,* 2017]. Thus, changes in
660 the charge potential of TCTE1 surface, which is one of the N-DRC components, seem to provide modified
661 (reduced) flagellar beating, similarly as in case of mutations in other N-DRC element – DRC4 protein, of which

662 changes in charge were essential for proper flagellar motility [Kubo *et al.,* 2017; Lewis *et al.,* 2016]. Also, the
663 inflexibility of the midpiece observed in spermatozoa of *Tcte1* knockout mice seems to be a consequence of
664 changed structure of LRRs in Tcte1 protein.

665 It is also known that the lengths of the sperm midpiece and tail may be crucial in determination of sperm
666 swimming velocity, followed then by decreased fertilization rate [Firman and Simmons 2010; Gu *et al.,* 2019].
667 Available data showed that sperm with shorter midpiece may swim slower and were observed in
668 asthenozoospermic cases [Firman and Simmons 2010; Gu *et al.,* 2019; Anderson *et al.,* 2002]. The meta-analysis
669 of sperm shape features according to sperm competition theory has also shown, that in majority of vertebrates
670 the longer sperm cell (including midpiece or flagellum) has been attributed to faster swimming, followed by the
671 statement that the sperm size may be increased when sperm number is lowered [Lüpold *et al.,* 2020]. In our
672 study we have documented longer sperm tails and midpieces in *Tcte1*$^{-/-}$ animals, that in fact were infertile. Thus,
673 we can suggest that: (i) the observed longer sperm tails and midpieces may be co-responsible for aberrant
674 motility observed, and (ii) the documented longer sperm tails and midpieces may be an indirect result of
675 constrained sperm count observed, because of some sort of compensation for aberrant motility. However, this
676 issue remains only a suggestion because of a restricted literature data relative to similar observations. Bennison
677 et al. [2016] revealed than in a passerine bird the sperm tail velocity was correlated to total sperm length, but
678 only to some point of the length value at which the velocity started to be decreased. On the other hand, Gu et
679 al. [2019] have shown that in mammalian species there were some changes in the axonemal slopes when the
680 flagellar length increases. The results obtained within our study, and supported by other research concerning
681 sperm tail beating pathways, should be a good start point for creation of further mathematical computations for
682 better understanding of the asthenozoospermia.

683 *Constrained energy metabolism*

684 The flagellar motility is determined by coordinated activity of asymmetrically distributed dyneins in the
685 axoneme. The driving factor for this activity is the hydrolysis of ATP released from OXPHOS system (Mitochondrial
686 Oxidative Phosphorylation System) [Tourmente *et al.,* 2015; Ford 2006]. ATP is being produced in mitochondria
687 placed within sperm midpiece. In our study ATP level measurements revealed its decreased level in sperm cells
688 of *Tcte1*$^{-/-}$ mice, what can result in faulty dynein functioning, leading to asthenozoospermia via abnormal sperm
689 tail beating. We have documented that *Tcte1* KO resulted in significant changes in expression level of testicular
690 genes involved in mitochondrial energy transport. That leads to the conclusion that homozygous *Tcte1* mutation

691 results not only in inflexible midpiece leading to asymmetric circular motility, as presented in this study and by
692 others [Fung *et al.,* 2018], and then to asthenozoospermia, but also to aberrant functioning of mitochondrial
693 OXPHOS machinery leading to disruption of ATP production. Thus, the sperm tail has also insufficient power for
694 beating because of the decreased ATP content. Castaneda et al. suggested that the reasons of the observed ATP
695 decrease may result from disturbances in a glycolytic pathway [Castaneda *et al.,* 2017]. It is already known, that
696 glycolytic energy is enough for spermatozoa to survive [Nascimento *et al.,* 2008; Zhang *et al.,* 2022]. However,
697 for sperm motility and then fertilization, the OXPHOS energy production is required [Tourmente *et al.,* 2015;
698 Ford 2006; Zhang *et al.,* 2022]. In our study, RNAseq results clearly revealed the influence of *Tcte1*$^{-/-}$ mutation on
699 genes involved directly in electron transport chain, such as: *mt-Co2* and *mt-Co3*, crucial components of the
700 respiratory chain complex IV, one of the OXPHOS elements. Observed reduced expression seems to clearly
701 evidence the decreased ATP production via disturbed electron chain transportation, and then revealing the
702 sperm motility reduction observed in *Tcte1*$^{-/-}$ males, leading to observed asthenozoospermia. Detailed STRING
703 analysis revealed definite interactions between both listed proteins identified in our study, and a list of other
704 mitochondrial ones (mt-Co1, mt-Cytb, Cox5a, Cox6a, Cox7c, mt-Atp6; Supplementary file 11; Supplementary file
705 12) clearly related to proper processing of cytochrome energetic activity [Brischigliaro and Zeviani 2021;
706 Ganetzky *et al.,* 2019]. Overexpression or mutations in *COX1*, *COX2*, and *COX3* were previously observed in
707 infertile men with varicocele and OAT, or diabetes [Heidari et al., 2016; Mostafa *et al.,* 2016; Perrotta *et al.,*
708 2012]. Additionally, it was shown that system of COX2 and prostaglandins plays key role in development of male
709 gonad, spermatogenesis and steroidogenesis, especially in functioning of Sertoli and Leydig cells, and also was
710 found to be significant in the background basis of idiopathic infertility status [Frungieri *et al.,* 2015]. It seems that
711 in our study the reason of observed disturbed motility, represented as circular movement of spermatozoa,
712 supported by increased ratio of immotile sperm cells in *Tcte*$^{-/-}$ mice, leading to asthenozoospermia, resulted from
713 two factors: (i) inflexibility of sperm midpiece resulted from changed protein charge level in the Tcte1 protein,
714 followed by elevated lengths of sperm tail and midpiece, and (ii) decreased amount of ATP produced, that may
715 be an outcome of inability to get sufficient energy for proper sperm motility.

716 *Protection and/or compensation?*

717 We have also documented an important role of the *Fetub* gene for the first time in the male testis.
718 Besides of its known role in female fertility [Karmilin *et al.,* 2019; Bansho *et al.,* 2017], the latest study pay
719 attention also in the context of prostate cancer is a detailed way [Zhan *et al.,* 2020]. It was found that

720 overexpression of *FETUB* increases the apoptosis of prostate cancer cells, followed by the inhibition of their
721 proliferation, migration and invasion, and also slower growth of tumor when compared to controls [Zhan *et al.,*
722 2020]. Thus, in the overexpression mode, the Fetub plays protective role for the prostate. It seems to explain
723 results obtained in our study, where the *Fetub* expression was increased almost 5-fold in *Tcte1*$^{-/-}$ mice, but no
724 tumor signs have been observed in the mouse testis at the tissue level. Zhan et al. [2020] have found the
725 connection between *Fetub* overexpression, and induction of Bax (Bcl-2-associated X protein) and capases,
726 resulting in promoting the apoptosis. It is known that the Bax/Bcl-2 induction/inhibition is directly related to the
727 release of cytochrome c (Cyt c) in the caspase-dependent signaling [Dadsena *et al.,* 2021; Samaiya *et al.,* 2021;
728 Li *et al.,* 2021]. And cytochrome c is one of the two electron carriers in electron transport chain responsible for
729 transport directly to the respiratory chain complex IV [Yin and O'Neil 2021; Alvarez-Paggi *et al.,* 2017]. Due to
730 Cyt c release, complex IV is essential for apoptosis and cell fate [Samaiya *et al.,* 2021; Li *et al.,* 2021]. Following
731 of all of those facts, our results seem to reveal the connection between *Fetub* and diminished mitochondrial
732 chain IV activity in mice testis, what have not been reported so far. It can be also supported by the fact of the
733 known relation between FETUB and the inactivation of the PI3K/AKT signaling pathway (key player in regulation
734 of cell proliferation and apoptosis in cancerogenesis), in which the Bax/Bcl-2 are involved [Zhan *et al.,* 2020].

735 The novel testis-protective role in our study can be also credited to three other genes with increased
736 expression level in testicular tissue: *Hoxd10* (3-fold increase), *Slc45a3* (2.2-fold), and *Ube2l* (2-fold).
737 Overexpression/activation of *HOXD10* has been already documented as inhibitor of tumorigenesis [Jonkers *et*
738 *al.,* 2020; Mo *et al.,* 2017; Zhang *et al.,* 2019]. Expression of *Slc45a3*, known also as 'prostein', has been
739 documented as weaker in cancer tissues [Hernández-Llodrà et al. 2017; Pin et al., 2017; Perner et al., 2013].
740 Elevated expression level of *Ube2l* is known to be connected with the degradation/suppression of tumor cells [Li
741 *et al.,* 2018]. On the other hand, the 12-fold increased gene expression level for *Usp39* (ubiquitin specific
742 peptidase 39) – an oncogenic splicing factor which expression is positively linked with cancerogenesis' promotion
743 in prostate or ovaries, while its silencing induces apoptosis and cell cycle arrest, has been noticed [Huang *et al.,*
744 2016; Yuan *et al.,* 2021; Zhao *et al.,* 2016].

745 Taken together data obtained for genes related to cancerogenesis and/or apoptosis described above,
746 we can hypothesize that we observe an interesting novel network of interactions between two groups of genes
747 that are reciprocally neutralizing potential influence onto the testis tissue. Mainly, in the first group we have
748 genes with suggested novel anti-cancer role in the testis (*Fetub*, *Hoxd10*, *Slc45a3, Ube2l6*), which increased

749 expression level inhibits the cancer cell development, supported by protective role of *Mt3*; while in the second
750 corner of the ring the *Usp39* gene with elevated expression level (the most from all the observed changes) should
751 lead to reveal some tumor-like changes within the testis tissue. Following the fact, that both: histological
752 evaluation, as well as caspase 3 staining (Fig.9), have shown no differences between hetero- and homozygous
753 mutant mice, our hypothesis seems to be justifiable. On the other hand, there is a prediction that many of the
754 genes (especially so-called cancer-testis associated antigens, CTA) related to spermatogenesis may function in
755 tumorigenesis [Aurriere *et al.,* 2021; Yang *et al.,* 2020; Babatunde *et al.,* 2017; Wang *et al.,* 2016; Bode *et al.,*
756 2014; Cheng *et al.,* 2011; Nagirnaja *et al.,* 2018]. Due to known similarities between oncogenic and
757 spermatogenic processes, especially in the energy metabolism, we can carefully suggest/hypothesize that in our
758 KO model the genes with changed expression profile found, known as highly involved in tumorigenesis, may also
759 be important in spermatogenesis. Obviously, there is a need for further studies in this direction to confirm these
760 suggestions or to reveal the other (still unknown) mechanisms.

761 *Conclusions*

762 We have documented that *TCTE1* gene is the next one that should be added to the 'male infertility list'
763 of molecular background because of its crucial role in spermatogenesis and proper sperm functioning. The
764 mutations in mouse *Tcte1* knockout model revealed two phenotypes, depending from zygosity with infertile
765 oligoasthenoteratozoospermic homozygotes, and fertile oligozoospermic heterozygotic males, suggesting
766 haploinsufficiency mechanism involvement. All collected data pointing that the Tcte1 protein is functioning in
767 spermatogenesis and show how its mutations add the level of complexity to the clinical manifestation of
768 decreased semen parameters. The disrupted energy machinery of the spermatozoa, followed by newly
769 suggested roles of genes related to cancerogenesis and/or apoptosis (here in the context of their
770 neutralizing/compensation effect on the testicular tissue), seem to underline the complex and devastating effect
771 of the single-gene mutation, on the variety of testicular molecular networks, leading to reproductive failure.

772

773 **ACKNOWLEDGEMENTS**

774 We are grateful to Oliwia Kordyl, MSc, and Katarzyna Kurek, MSc (IHG PAS, Poznan) for their technical help in
775 preparation of the samples for sequencing, genotyping, and immunofluorescence staining.

776

777

Authors' contributions:

MO design of the study, manuscript drafting and editing, coordination of the tasks, data interpretation, gene selection, preparation of human blood and semen samples, mice: mating, genotyping, gross sections and preparation of biological samples, RNAseq analysis, immunofluorescence, Sanger sequencing, ATP measurements; **AM** gene selection, data interpretation, genotyping, RNAseq analysis, collection and preparation of human testis samples, WGS and Sanger sequencing, manuscript editing; **TS** bioinformatic analysis of RNAseq and WGS results; **NP** WES of azoospermia samples (incl. bioinformatics); **AB** protein prediction modeling and its description; **SB** preparation of: DNA for sequencing, RNA for RNAseq, screening of databases for RNAseq results; **MKa** collection of human blood and semen samples, semen analyses of human and mouse samples, detailed morphology of mouse spermatozoa; **HJ** histopathology of mouse tissue sections; **PJ** recruitment of patients and their medical history; **ANY** gene selection, interpretation of azoospermia WES results, data interpretation; **MKu** data interpretation, gene selection, recruitment of patients and their medical history, correction of the manuscript, funds collection and supervision.

All authors critically reviewed and approved the final version of the manuscript.

LARGE SCALE DATA: All data generated or analyzed during this study are included in this published article and its supplemental information files.

RNAseq data are available in GEO database (https://www.ncbi.nlm.nih.gov/geo/) under the accession number: GSE207805.

The results described in the publication are based on whole-genome or exome sequencing data which includes sensitive information in the form of patient specific germline variants. Information regarding such variants must not be shared publicly following the European Union legislation described in the following document: https://publications.jrc.ec.europa.eu/repository/bitstream/JRC113479/policy_report_-_review_of_eu_national_legislation_on_genomics_-_with_identifiers_1.pdf, therefore the access to raw data that support findings of this study are available from the corresponding author upon reasonable request.

LIMITATIONS, REASONS FOR CAUTION: In the study, the *in vitro* fertilization ability of homozygous male mice was not checked.

WIDER IMPLICATIONS OF THE FINDINGS: This study contains novel and the most complete data concerning *TCTE1* role in male infertility. *TCTE1* gene is the next one that should be added to the 'male infertility list' of molecular background because of its crucial role in spermatogenesis and proper sperm functioning.

STUDY FUNDING/COMPETING INTEREST(S): This work was supported by National Science Centre in Poland, grants no.: 2015/17/B/NZ2/01157 and 2020/37/B/NZ5/00549 (to MK), 2017/26/D/NZ5/00789 (to AM), and HD096723, GM127569-03, NIH SAP #4100085736 PA DoH (to AY). The authors declare that there is no conflict of interest that could be perceived as prejudicing the impartiality of the research reported.

813 **REFERENCES**

814

815 Agarwal A, Baskaran S, Parekh N, Cho CL, Henkel R, Vij S, Arafa M, Panner Selvam MK, Shah R. Male infertility.
816 *Lancet* 2021;**397**: 319-333 https://doi.org/10.1016/S0140-6736(20)32667-2
817 Alvarez-Paggi D, Hannibal L, Castro MA, Oviedo-Rouco S, Demicheli V, Tórtora V, Tomasina F, Radi R, Murgida
818 DH. Multifunctional Cytochrome c: Learning New Tricks from an Old Dog. *Chem Rev* 2017;**117**:13382-13460
819 https://doi.org/10.1021/acs.chemrev.7b00257
820 Anderson MJ, Dixson A F. Sperm competition: motility and the midpiece in primates. *Nature* 2002;**416**:496
821 https://doi.org/10.1038/416496a
822 Aprea I, Raidt J, Höben M, Loges NT, Nöthe-Menchen T, Pennekamp P, Olbrich H, Kaiser T, Biebach L, Tüttelmann
823 F. et al. Aprea I, et al. Defects in the cytoplasmic assembly of axonemal dynein arms cause morphological
824 abnormalities and dysmotility in sperm cells leading to male infertility. *PloS Genet* 2021;17:e1009306
825 https://doi.org/10.1371/journal.pgen.1009306
826 Aurrière J, Goudenège D, Baris OR, Boguenet M, May-Panloup P, Lenaers G, Khiati S. Cancer/Testis Antigens into
827 mitochondria: a hub between spermatogenesis, tumorigenesis and mitochondrial physiology adaptation.
828 *Mitochondrion* 2021;**56**:73-81 https://doi.org/10.1016/j.mito.2020.11.002
829 Babatunde KA, Najafi A, Salehipour P, Modarressi MH, Mobasheri MB. Cancer/Testis genes in relation to sperm
830 biology and function. *Iran J Basic Med Sci* 2017;**20**:967-974 https://doi.org/10.22038/IJBMS.2017.9259
831 Baklouti-Gargouri S, Ghorbel M, Mahmoud AB, Mkaouar-Rebai E, Cherif M, Chakroun N, Sellami A, Fakhfakh F,
832 Ammar-Keskes L. Mitochondrial DNA mutations and polymorphisms in asthenospermic infertile men. *Mol Biol*
833 *Rep* 2013;**40**:4705–4712 https://doi.org/10.1007/s11033-013-2566-7
834 Bansho Y, Lee J, Nishida E, Nakajima-Koyama M. Identification and characterization of secreted factors that are
835 upregulated during somatic cell reprogramming. *FEBS Letters* 2017;**591**:1584-1600
836 https://doi.org/10.1002/1873-3468.12665
837 Barratt CLR, Björndahl L, De Jonge CJ, Lamb DJ, Martini FO, McLachlan R, Oates RD, van der Poel S, St John B,
838 Sigman M, et al. The diagnosis of male infertility: an analysis of the evidence to support the development of
839 global WHO guidance-challenges and future research opportunities. *Hum Reprod Update* 2017;**23**:660-680
840 https://doi.org/10.1093/humupd/dmx021

841 Bennison C, Hemmings N, Brookes L, Slate J, Birkhead T. Sperm morphology, adenosine triphosphate (ATP)
842 concentration and swimming velocity: unexpected relationships in a passerine bird. Proc. Royal Soc. B -Biol Sci
843 2016;**283**:20161558 https://doi.org/10.1098/rspb.2016.1558
844 Binsila BK, Archana SS, Ramya L, · Swathi D, · Selvaraju S, Shivakumar Gowda NKS, · Pal DT, · Rafay A,· Bhattaet R.
845 Elucidating the processes and pathways enriched in buffalo sperm proteome in regulating semen quality. Cell
846 Tissue Res 2021;**383**:881-903 https://doi.org/10.1007/s00441-020-03303-9
847 Bode PK, Thielken A, Brandt S, Barghorn A, Lohe B, Knuth A, Moch H. Cancer testis antigen expression in testicular
848 germ cell tumorigenesis. *Modern Pathology* 2014;**27**: 899-905 https://doi.org/10.1038/modpathol.2013
849 Bower R, Tritschler D, VanderWaal Mills K, Heuser T, Nicastro D, Porter ME. DRC2/CCDC65 is a central hub for
850 assembly of the nexin-dynein regulatory complex and other regulators of ciliary and flagellar motility. *Mol Biol*
851 *Cell* 2018;**29**:137-153 https://doi.org/10.1091/mbc.E17-08-0510
852 Brischigliaro M, Zeviani M. Cytochrome c oxidase deficiency. *Biochim Biophys Acta - Bioenerg* 2021;**1862**: 148335
853 https://doi.org/10.1016/j.bbabio.2020.148335
854 Cai J, Huang H, Hu X, Lang W, Fu W, Xu L, Qiu Z, Zhong H, Chen F. Homoharringtonine Synergized with Gilteritinib
855 Results in the Downregulation of Myeloid Cell Leukemia-1 by Upregulating UBE2L6 in FLT3-ITD-Mutant Acute
856 Myeloid (Leukemia) Cell Lines. *J Oncol* 2021, 3766428 https://doi.org/10.1155/2021/3766428
857 Cannarella R, Condorelli RA, La Vignera S, Bellucci C, Luca G, Calafiore R, Calogeroet AE. IGF2 and IGF1R mRNAs
858 Are Detectable in Human Spermatozoa. *World J Mens Health* 2020;**38**:545-551
859 https://doi.org/10.5534/wjmh.190070
860 Castaneda JM, Hua R, Miyata H, Oji A, Guo Y, Cheng Y, Zhou T, Guo X, Cui Y, Shen B, et al. TCTE1 is a conserved
861 component of the dynein regulatory complex and is required for motility and metabolism in mouse spermatozoa.
862 *PNAS* 2017;**114**,E5370-E5378 https://doi.org/10.1073/pnas.1621279114
863 Chemes HE, Olmedo SB, Carrere C, Oses R, Carizza C, Leisner M, Blaquier J. Ultrastructural pathology of the
864 sperm flagellum: association between flagellar pathology and fertility prognosis in severely asthenozoospermic
865 men. *Hum Reprod* 1998;**13**:2521-2526 https://doi.org/10.1093/humrep/13.9.2521
866 Chen Y, Wang J, Pan C, Li D, Han X. Microcystin-leucine-arginine causes blood-testis barrier disruption and
867 degradation of occludin mediated by matrix metalloproteinase-8. *Cell Molecukar Life Sci* 2018;**75**:1117-1132
868 https://doi.org/10.1007/s00018-017-2687-6

869 Cheng YH, Wong EWP, Cheng CY. Cancer/testis (CT) antigens, carcinogenesis and spermatogenesis.
870 *Spermatogenesis* 2011;**1**:209-220 https://doi.org/10.4161/spmg.1.3.17990
871 Chiang C, Layer RM, Faust GG, Lindberg MR, Rose DB, Garrison EP, Marth GT, Quinlan AR, Hall IM. SpeedSeq:
872 Ultra-fast personal genome analysis and interpretation. *Nat Methods* 2015;**12**:966-968
873 https://doi.org/10.1038/nmeth.3505.
874 Dadsena S, King LE, Garcia-Saez AJ. Apoptosis regulation at the mitochondria membrane level. *Biochim Biophys*
875 *Acta – Biomembranes* 2021;**1863**:183718 https://doi.org/10.1016/j.bbamem.2021.183716
876 Damaschke NA, Yang B, Bhusari S, Avilla M, Zhong W, Blute ML, Huang W, Jarrard DF. Loss of Igf2 Gene Imprinting
877 in Murine Prostate Promotes Widespread Neoplastic Growth. Cancer Res 2017;**77**:5236-5247
878 https://doi.org/10.1158/0008-5472.CAN-16-3089
879 Drechsler H, Xu Y, Geyer VF, Zhang Y, Diez S. Multivalent electrostatic microtubule interactions of synthetic
880 peptides are sufficient to mimic advanced MAP-like behavior. *Mol Biol Cell* 2019;**30**:2953-2968
881 https://doi.org/10.1091/mbc.E19-05-0247
882 Du Plessis SS, Gokul S, Agarwal A. Semen hyperviscosity: causes, consequences, and cures. *Front Biosci (Elite Ed)*
883 2013;**5**:224-231 https://doi.org/10.2741/E610
884 Emsley P, Lohkamp B, Scott WG, Cowtan K. Features and development of Coot. *Acta Crystallogr D Struct Biol*
885 2010;**66**:486-501 https://doi.org/10.1107/S0907444910007493
886 Fink E, Bhoola KD, Snyman C, Neth P, Figueroa CD. Cellular expression of plasma prekallikrein in human tissues.
887 *Biol Chem* 2007;**388**:957-963 https://doi.org/10.1515/BC.2007.104
888 Firman RC, Simmons L. W. Sperm midpiece length predicts sperm swimming velocity in house mice. Biol Letters
889 2010;**6**:513-516 https://doi.org/10.1098/rsbl.2009.1027
890 Ford WC. Glycolysis and sperm motility: does a spoonful of sugar help the flagellum go round? Hum Reprod
891 Update 2006;12:269-274 https://doi.org/10.1093/humupd/dmi053
892 Frungieri MB, Calandra RS, Mayerhofer A, Matzkin ME. Correlation between testicular mast cell count and
893 spermatogenic epithelium in non-obstructive azoospermia. *Reproduction* 2015;**149**:R169-R180
894 https://doi.org/10.1111/iep.12261
895 Fung E, Richter C, Yang HB, Schäffer I, Fischer R, Kessler BM, Bassermann F, D'Angiolella V. FBXL13 directs the
896 proteolysis of CEP192 to regulate centrosome homeostasis and cell migration. *EMBO Rep* 2018;**19**:e44799
897 https://doi.org/10.15252/embr.201744799

898 Ganetzky RD, Stendel C, McCormick EM, Zolkipli-Cunningham Z, Goldstein AC, Klopstock T, Falk MJ. MT-ATP
899 mitochondrial disease variants: phenotypic and biochemical features analysis in 218 published cases and cohort
900 of 14 new cases. *Hum Mutation* 2019;**40**:499-515 https://doi.org/10.1002/humu.23723
901 Gao Y, Hong J, Guo Y, Chen M, Chang AK, Xie L, Ying X. Assessment spermatogenic cell apoptosis and the
902 transcript levels of metallothionein and p53 in Meretrix meretrix induced by cadmium. *Ecotoxicol Environ Saf*
903 2021;**217**:112230 https://doi.org/10.1016/j.ecoenv.2021.112230
904 Ghosh D, Najwa AR, Khan MA, Sengupta J. IGF2, IGF binding protein 1, and matrix metalloproteinases 2 and 9 in
905 implantation-stage endometrium following immunoneutralization of vascular endothelial growth factor in the
906 rhesus monkey. *Reproduction* 2011;**141**:501-509 https://doi.org/10.1530
907 Girardet L, Augière C, Asselin MP, Belleannée C. Primary cilia: biosensors of the male reproductive tract.
908 *Andrology* 2019;7:588-602 https://doi.org/10.1111/andr.12650
909 Gu NH, Zhao WL, Wang GS, Sun F. Comaprative analysis of mammalian sperm ultrastructure reveals relationships
910 between sperm morphology, mitochondrial functions and motility. *Reprod Biol Endocrinol* 2019;**17**:66
911 https://doi.org/10.1186/s12958-019-0510-y
912 Gui L, Song K, Tritschler D, Bower R, Yan S, Dai A, Augspurger K, Sakizadeh J, Grzemska M, Ni T, et al. Scaffold
913 subunits support associated subunit assembly in the Chlamydomonas ciliary nexin-dynein regulatory complex.
914 *Proc Natl Acad Sci USA* 2019;**116**:23152-23162 https://doi.org/10.1073/pnas.1910960116
915 Ha S, Lindsay AM, Timms AE, Beier DR. Mutations in Dnaaf1 and Lrrc48 Cause Hydrocephalus, Laterality Defects,
916 and Sinusitis in Mice. *G3* 2016;**6**:2479-2487 https://doi.org/10.1534/g3.116.030791
917 Hardy JJ, Wyrwoll MJ, Mcfadden W,· Malcher A,· Rotte N, · Pollock NC, Munyoki S, Veroli MV, Houston BJ, · Miguel
918 J et al. XavierVariants in GCNA, X-linked germ-cell genome integrity gene, identified in men with primary
919 spermatogenic failure. *Hum Genet* 2021;140:1169-1182 https://doi.org/10.1007/s00439-021-02287-y
920 Heidari MM, Khatami M, Danafar A, Dianat T, Farahmand G, Talebi AR. 4Mitochondrial Genetic Variation in
921 Iranian Infertile Men with Varicocele. *Int J Fertil Steril* 2016;**10**:303-309 doi: 10.22074/ijfs.2016.5047.
922 Hernández-Llodrà S, Juanpere N, de Muga S, Lorenzo M, Gil J, Font-Tello A, Agell L, Albero-González R, Segalés L,
923 Merino J, et al. ERG overexpression plus SLC45A3 (prostein) and PTEN expression loss: Strong association of the
924 triple hit phenotype with an aggressive pathway of prostate cancer progression. *Oncotarget* 2017;**8**:74106-74118
925 https://doi.org/10.18632/oncotarget.18266

926 Heshusius, S, Grech L, Gillemans N, Brouwer RWW, den Dekker XT, van IJcken WFJ, Nota B, Felice AE, van Dijk
927 TB, von Lindern M, et al. Epigenomic analysis of KLF1 haploinsufficiency in primary human erythroblasts. *Sci Rep*
928 2022;**12**:336 https://doi.org/10.1038/s41598-021-04126-6
929 Heuser T, Raytchev M, Krell J, Porter ME, Nicastro D. The dynein regulatory complex is the nexin link and a major
930 regulatory node in cilia and flagella. *J Cell Biol* 2009;**187**:921-933 https://doi.org/10.1083/jcb.200908067
931 Honda A, Komuro H, Shimada A, Hasegawa T, Seko Y, Nagase H, Hozumi I, Inuzuka T, Hara H, Fujiwara Y, et al.
932 Attenuation of cadmium-induced testicular injury in metallothionein-III null mice. *Life Sci* 2010;**87**:545-550
933 https://doi.org/10.1016/j.lfs.2010.09.009
934 Houston BJ, Riera-Escamilla A, Wyrwoll MJ, Salas-Huetos A, Xavier MJ, Nagirnaja L,Friedrich C, Conrad DF, Aston
935 AI, Krausz C et al. A systematic review of the validated monogenic causes of human male infertility: 2020 update
936 and a discussion of emerging gene–disease relationships. *Hum Reprod Update* 2021;28:15-29
937 https://doi.org/10.1093/humupd/dmab030
938 Huang Y, Huang Y, Pan XW, Li L, Lu Chen, Liu X, Lu JL, Zhu XM, Huang H, Yang QW, Ye JQ et al. Overexpression of
939 USP39 predicts poor prognosis and promotes tumorigenesis of prostate cancer via promoting EGFR mRNA
940 maturation and transcription elongation. *Oncotarget* 2016;**7**:22016-22030
941 https://doi.org/10.18632/oncotarget.7882
942 Hull RL, Johnson PY, Braun KR, Day AJ, Wight TN. Hyaluronan and hyaluronan binding proteins are normal
943 components of mouse pancreatic islets and are differentially expressed by islet endocrine cell types. *J Histochem*
944 *Cytochem* 2021;**60**:749-760 https://doi.org/10.1369/002215541245704
945 Hwang K, Smith JF, Coward RM, Penzias A, Bendikson K, Butts S, Coutifaris C, Falcone T, Fossum G, Gitlin S et al
946 (Practice Committee of the American Society for Reproductive Medicine in collaboration with the Society for
947 Male Reproduction and Urology) Evaluation of the azoospermic male: a committee opinion. *Fertil Steril*
948 2018;109:777-782 https://doi.org/10.1016/j.fertnstert.2018.01.043
949 Ioannidis NM, Rothstein JH, Pejaver V, Middha S, McDonnell SK, Baheti S, Musolf A, Li Q, Holzinger E, Karyadi D,
950 et al. REVEL: An Ensemble Method for Predicting the Pathogenicity of Rare Missense Variants. *Am J Hum Genet*
951 2016;**99**:877-885 https://doi.org/10.1016/j.ajhg.2016.08.016
952 Ishikawa T. Axoneme structure from motile cilia. *Cold Spring Harbor Perspectives in Biology* 2017;**9**,a028076
953 https://doi.org/10.1101/cshperspect.a028076

954 Jia Y, Ohanyan A, Lue YH, Swerdloff RS, Liu PY, Cohen P, Wang C. The effects of humanin and its analogues on
955 male germ cell apoptosis induced by chemotherapeutic drugs. *Apoptosis* 2015;**20**:551-561
956 https://doi.org/10.1007/s10495-015-1105-5
957 Jodar M, Oliva R. Protamine alterations in human spermatozoa. *Adv Exp Med Biol* 2014;**791**:83-102
958 https://doi.org/10.1007/978-1-4614-7783-9_6
959 Jonkers J, Pai P, Sukumar S. Multiple roles of HOX proteins in Metastasis: Let me count the ways. *Cancer*
960 *Metastasis Rev* 2020;**39**:661-679 https://doi.org/10.1007/s10555-020-09908-4
961 Jumper J Evans R, Pritzel A, Green T, Figurnov M, Ronneberger O, Tunyasuvunakool K, Bates R, Žídek A, Potapenko
962 A et al. Highly accurate protein structure prediction with AlphaFold. *Nature* 2021;**596**:583-589
963 https://doi.org/10.1038/s41586-021-03819-2
964 Karmilin K, Schmitz C, Kuske M, Körschgen H, Olf M, Meyer K, Hildebrand A, Felten M, Fridrich S, Yiallouros I, et
965 al. Mammalian plasma fetuin-B is a selective inhibitor of ovastacin and meprin metalloproteinases. *Sci Rep*
966 2019;**9**:546 https://doi.org/10.1038/s41598-018-37024-5
967 Kelley LA, Mezulis S, Yates CM, Wass MN, Sternberg MJ. The Phyre2 web portal for protein modeling, prediction
968 and analysis. *Nat Protoc* 2015;**10**:845-858 https://doi.org/10.1038/nprot.2015.053.
969 Khelifa MB, Coutton C, Zouari R, Karaouzène T, J, Bidart, M, Yassine SV, Delaroche J, Hennebicq S, et al. Mutations
970 in DNAH1, which encodes an inner arm heavy chain dynein, lead to male infertility from multiple morphological
971 abnormalities of the sperm flagella. *Am J Hum Genet* 2014;**94**:95-104
972 http://dx.doi.org/10.1016/j.ajhg.2013.11.017
973 Kherraf ZE, Christou-Kent M, Karaouzene T, Amiri-Yekta A, Martinez G, S Vargas AS, Lambert E, Borel C, Dorphin
974 B, Aknin-Seiferet I, et al. SPINK2 deficiency causes infertility by inducing sperm defects in heterozygotes and
975 azoospermia in homozygotes. *EMBO Mol Med* 2017;**9**:1132-1149 https://doi.org/10.15252/emmm.201607461
976 Klein C, Troedsson MHT, Rutllant J. Region-Specific Expression of Aquaporin Subtypes in Equine Testis,
977 Epididymis, and Ductus Deferens. *Anatomical Records (Hoboken)* 2013;**296**:1115-1126
978 https://doi.org/10.1002/ar.22709
979 Kobe B, Kajava AV. The leucine-rich repeat as a protein recognition motif. *Curr Opin Struct Biol* 2001;**11**:725-732
980 https://doi.org/10.1016/S0959-440X(01)00266-4
981 Krausz C, Riera-Escamilla A. Genetics of male infertility. *Nat Rev Urol* 2018;15: 369-384
982 https://doi.org/10.1038/s41585-018-0003-3

983 Krissinel E, Henrick K. Secondary-structure matching (SSM), a new tool for fast protein structure alignment in
984 three dimensions. *Acta Crystallogr D Biol Crystallogr* 2004;**60**:2256-2268
985 https://doi.org/10.1107/S0907444904026460
986 Kubo T, Oda T. Electrostatic interaction between polyglutamylated tubulin and the nexin-dynein regulatory
987 complex regulates flagellar motility. *Mol Biol Cell* 2017;**28**:2260-2266 https://doi.org/10.1091/mbc.e17-05-0285
988 Kumar D. Reiter J. How the centriole builds its cilium: of mothers, daughters, and the acquisition of appendages.
989 *Curr Opin Strucl Biol* 2021;66:41-48 https://doi.org/10.1016/j.sbi.2020.09.006
990 Leal LF, Szarek E, Berthon A, Nesterova M, Faucz FR, London E, Mercier C, Abu-Asab M, Starost MF, Dye L, et al.
991 Pde8b haploinsufficiency in mice is associated with modest adrenal defects, impaired steroidogenesis, and male
992 infertility, unaltered by concurrent PKA or Wnt activation. *Mol Cellular Endocrinol* 2021;**522**:111117
993 https://doi.org/10.1016/j.mce.2020.111117
994 Lei Q, Huanga X, Zhenga L, Zhenga F, Donga J, Chena F, Zeng W. Biosensors for Caspase-3: From chemical
995 methodologies to biomedical applications. *Talanta* 2022;240:123198
996 https://doi.org/10.1016/j.talanta.2021.123198
997 Lewis WR, Malarkey EB, Tritschler D, Bower R, Pasek RC, Porath JD, Birket SE, Saunier S, Antignac C, Knowles MR,
998 et al. Mutation of Growth Arrest Specific 8 Reveals a Role in Motile Cilia Function and Human Disease. *PLoS Genet*
999 2016;**12**:e1006220 https://doi.org/10.1371/journal.pgen.1006220
1000 Li H, Xing L, Zhao N, Wang J, Zheng N. Furosine Induced Apoptosis by the Regulation of STAT1/STAT2 and
1001 UBA7/UBE2L6 Genes in HepG2 Cells. *Int J Mol Sci* 2018;**19**:1629 https://doi.org/10.3390/ijms19061629
1002 Li K, van Delft MF, Dewson G. Too much death can kill you: inhibiting intrinsic apoptosis to treat disease. *EMBO*
1003 *J* 2021;**40**:e107341 https://doi.org/10.15252/embj.2020107341
1004 Lorès P, Kherraf ZE, Amiri-Yekta A, Whitfeld M, Daneshipour A, Stouvenel L, Cazin C, Cavarocchi E, Coutton C,
1005 Llabador MA et al. A missense mutation in IFT74, encoding for an essential component for intraflagellar transport
1006 of Tubulin, causes asthenozoospermia and male infertility without clinical signs of Bardet-Biedl syndrome. *Hum*
1007 *Genet* 2021;**140**:1031-1043 https://doi.org/10.1007/s00439-021-02270-7
1008 Lue Y, Swerdloff R, Jia Y, Wang C. The emerging role of mitochondrial derived peptide humanin in the testis.
1009 *Biochim Biophys Acta Gen Subj* 2021;**1865**:130009 https://doi.org/10.1016/j.bbagen.2021.130009

1010 Lüpold S, de Boer RA, Evans JP, Tomkins JL, Fitzpatrick JL. How sperm competition shapes the evolution of testes
1011 and sperm: a meta-analysis. *Philos Trans R Soc Lond B Biol Sci* 2020;**375**:20200064
1012 https://doi.org/10.1098/rstb.2020.0064
1013 Markou, A, Unger L, Abir-Awan M, Saadallah A, Halsey A, Baklava Z, Conner M, Törnroth-Horsefield S, Greenhill
1014 SD, Alex Conneret A, et al. Molecular mechanisms governing aquaporin relocalisation. *Biochim Biophys Acta –*
1015 *Biomembr* 2022;**1864**:183853 https://doi.org/10.1016/j.bbamem.2021.183853
1016 Marques PI, Fonseca F, Carvalho AS, Puente DA, Damião I, Almeida V, Barros N, Barros A, Carvalho F, Azkargortaet
1017 M et al. Sequence variation at KLK and WFDC clusters and its association to semen hyperviscosity and other male
1018 infertility phenotypes. *Hum Reprod* 2016;**31**:2881-2891 https://doi.org/10.1093/humrep/dew267
1019 Martinez G, Coutton C, Loeuillet C, Cazin C, Muroňová J, Boguenet M, Lambert E, Dhellemmes M, Chevalier G,
1020 Hograindleur JP et al. Oligogenic heterozygous inheritance of sperm abnormalities in mouse. *Elife*
1021 2022;**11**:e75373 https://doi.org/10.7554/eLife.75373
1022 Matsushima N, Takatsuka S, Miyashita H, Kretsinger RH. Leucine rich repeat proteins: sequences, mutations,
1023 structures and diseases. *Protein Pept Lett* 2019;**26**:108-131
1024 https://doi.org/10.2174/0929866526666181208170027
1025 Matsuzaki, H., Hitomi Matsuzaki, Kuramochi D, Okamura E, Hirakawa K, Ushiki A, Tanimoto K. Recapitulation of
1026 gametic DNA methylation and its post-fertilization maintenance with reassembled DNA elements at the mouse
1027 Igf2/H19 locus. *Epigenetics Chromatin* 2020:**13**:2 https://doi.org/10.1186/s13072-019-0326-1
1028 Matzuk MM, Lamb DJ. The biology of infertility: research advances and clinical challenges. *Nat Med*
1029 2008;14:1197-1213 https://doi.org/10.1038/nm.f.1895
1030 McLaren W, Gil L, Hunt SE, Riat HS, Ritchie GRS, Thormann A, Flicek P, Cunningham F. The Ensembl Variant Effect
1031 Predictor. *Genome Biol* 2016;**17**:122 https://doi.org/10.1186/s13059-016-0974-4
1032 Mei S, Wu Y, Wang Y, Cui Y, Zhang M, Zhang T, Huang X, Yu S, Yu T. Disruption of PIKFYVE causes congenital
1033 cataract in human and zebrafish. *Elife* 2022;**11**:e71256 https://doi.org/10.7554/eLife.71256
1034 Michaelis M, Sobczak A, Koczan D, Langhammer M, Reinsch N, Schoen J, WeitzeL JM. Selection for female traits
1035 of high fertility affects male reproductive performance and alters the testicular transcriptional profile. *BMC*
1036 *Genomics* 2017;**18**:889 https://doi.org/10.1186/s12864-017-4288-z

1037 Mo RJ, Lu JM, Wan YP, Hua W, Liang YX, Zhuo YJ, Kuang QW, Liu YL, He HC, Zhong WD. Decreased HoxD10
1038 Expression Promotes a Proliferative and Aggressive Phenotype in Prostate Cancer. *Curr Mol Med* 2017;**17**:70-78
1039 https://doi.org/10.2174/1566524017666170220104920
1040 Morohoshii A, Miyataid H, Shimadaid K, Nozawa K, Matsumura T, Yanaseid R, Shibaid K, Inabaid K, Ikawa M.
1041 Nexin-dynein regulatory complex component DRC7 but not FBXL13 is required for sperm flagellum formation
1042 and male fertility in mice. *PloS Genet* 2020;**16**:e1008585 https://doi.org/10.1371/journal.pgen.1008585
1043 Mostafa T, Rashed L, Taymour M. Seminal cyclooxygenase relationship with oxidative stress in infertile
1044 oligoasthenoteratozoospermic men with varicocele. *Andrologia* 2016;**48**:137142
1045 https://doi.org/10.1111/and.12423
1046 Nagirnaja L, Aston KI, Conrad DF. Genetic intersection of male infertility and cancer. *Fertil Steril* 2018;**109**:20-26
1047 https://doi.org/10.1016/j.fertnstert.2017.10.028
1048 Nascimento JM, Shi LZ, Tam J, Chandsawangbhuwana C, Durrant B, Botvinick EL, Berns MW. Comparison of
1049 glycolysis and oxidative phosphorylation as energy sources for mammalian sperm motility, using the combination
1050 of fluorescence imaging, laser tweezers, and real-time automated tracking and trapping. *J Cell Physiol*
1051 2008;**217**:745-51 https://doi.org/10.1002/jcp.21549
1052 Naz RK, Rajesh C. Gene knockouts that cause female infertility: search for novel contraceptive targets. *Front*
1053 *Biosci* 2005;**10**:2447-2459 https://doi.org/10.2741/1709
1054 Neirijnck Y, Kühne F, Mayère C, Pavlova E, Sararols P, Foti M, Atanassova N, Nef S. Tumor Suppressor PTEN
1055 Regulates Negatively Sertoli Cell Proliferation, Testis Size, and Sperm Production In Vivo. *Endocrinology*
1056 2019;**160**:387-398 https://doi.org/10.1210/en.2018-00892
1057 Ng ACY, Eisenberg JM, Heath RJ, Huett A, Robinson CM, Nau GJ, Xavier RJ. Human leucine-rich repeat proteins:
1058 a genome-wide bioinformatic categorization and functional analysis in innate immunity. *Prot Nat Acad Sci*
1059 2011;**108**:4631-4638 https://doi.org/10.1073/pnas.100009310
1060 Ogura, Y., Uehara T, Ujibe K, Yoshihashi H, Yamada M, Suzuki H, Takenouchi T, Kosaki K, Hirata H. The
1061 p.Thr395Met missense variant of NFIA found in a patient with intellectual disability is a defective variant.
1062 *American Journal of Medical Genetics A* 2022;**188**:1184-1192 https://doi.org/10.1002/ajmg.a.62638
1063 Oud MS, Houston BJ, Volozonoka L, Mastrorosa FK, Holt GS, Alobaidi BKS, deVries PF, Astuti G, Ramos L,
1064 Mclachlan RI et al. Exome sequencing reveals variants in known and novel candidate genes for severe sperm
1065 motility disorders. *Hum Reprod* 2021;36:2597-2611 https://doi.org/10.1093/humrep/deab099

1066 Pan W, Wang K, Li J, Li H, Cai Y, Zhang M, Wang A, Wu Y, Gao W, Weng W. 1Restoring HOXD10 Exhibits
1067 Therapeutic Potential for Ameliorating Malignant Progression and 5-Fluorouracil Resistance in Colorectal Cancer.
1068 *Front Oncol* 2021;**11**:771528 https://doi.org/10.3389/fonc.2021.771528
1069 Perner S, Rupp NJ, Braun M, Rubin MA, Moch H, Dietel M, Wernert N, Jung K, Stephan C, Kristiansen G. Loss of
1070 SLC45A3 protein (prostein) expression in prostate cancer is associated with SLC45A3-ERG gene rearrangement
1071 and an unfavorable clinical course. *Int J Cancer* 2013;132;807-812 https://doi.org/10.1002/ijc.27733
1072 Perrotta I, Santoro M, Guido C, Avena P, Tripepi S, De Amicis F, Gervasi MC, Aquila S. Expression of
1073 cyclooxygenase-1 (COX-1) and COX-2 in human male gametes from normal patients, and those with varicocele
1074 and diabetes: a potential molecular marker for diagnosing male infertility disorders. *J Anat* 2012;**221**:209-220
1075 https://doi.org/10.1111/j.1469-7580.2012.01534.x
1076 Pin E, Frauke Henjes F, Hong MG, Wiklund F, Patrik Magnusson P, Anders Bjartell A, Uhlen M, Nilsson P, Schwenk
1077 JM. Identification of a Novel Autoimmune Peptide Epitope of Prostein in Prostate Cancer. *J Proteome Res*
1078 2017;**16**:04-216 https://doi.org/10.1021/acs.jproteome.6b00620
1079 Ramli NSK, Giribabu N, Karim K, Salleh N. Hormonal control of vas deferens fluid volume and aquaporin
1080 expression in rats. *J Mol Histol* 2019;**50**:21-34 https://doi.org/10.1007/s10735-018-9804-1
1081 Richards S, Aziz N, Sherri Bale S, Bick D, Das S, Gastier-Foster J, Grody WW, Hegde M P, Lyon E, Spector E, et al.
1082 Standards and guidelines for the interpretation of sequence variants: a joint consensus recommendation of the
1083 American College of Medical Genetics and Genomics and the Association for Molecular Pathology. *Genet Med*
1084 2015;**17**:405-424 https://doi.org/doi:10.1038/gim.2015.30
1085 Romeis B, Mulisch M, Welsch U. Romeis Mikroskopische Technik. Dordrecht: Springer. 2010; xii, 550 s. p.
1086 Roy A, Kucukural A, Zhang Y. I-TASSER: a unified platform for automated protein structure and function
1087 prediction. *Nat Protoc* 2010;**5**:725-738 https://doi.org/10.1038/nprot.2010.5
1088 Salustri A, Campagnolo L, Klinger FG, Camaioni A. Molecular organization and mechanical properties of the
1089 hyaluronan matrix surrounding the mammalian oocyte. *Matrix Biol* 2019;78-79:11-23
1090 https://doi.org/10.1016/j.matbio.2018.02.002
1091 Samaiya PK, Krishnamurthy S, Kumar A. Mitochondrial dysfunction in perinatal asphyxia: role in pathogenesis
1092 and potential therapeutic interventions. *Mol Cell Biochem* 2021;**476**:4421-4434 https://doi.org/10.1007/s11010-
1093 021-04253-8

1094 Sandhu N, Rana S, Meena K. Nuclear receptor subfamily 5 group A member 2 (NR5A2): role in health and
1095 diseases. *Mol Biol Rep* 2021;**48**:8155-8170 https://doi.org/10.1007/s11033-021-06784-1
1096 Sandy Z, da Costa IC, Schmidt CK. More than Meets the ISG15: Emerging Roles in the DNA Damage Response and
1097 Beyond. *Biomolecules* 2020;**10**:1557 https://doi.org/10.3390/biom10111557
1098 Satir P, Heuser T, Sale WS. A structural basis for how motile cilia beat. *Bioscience* 2014;**64**:1073-1083
1099 https://doi.org/10.1093/biosci/biu180
1100 Sato JD, Kan M. Media for culture of mammalian cells. *Curr Protoc Cell Biol* 2001; Chapter 1:Unit 1.2.
1101 Schlegel PN, Sigman M, Collura B, De Jonge CJ, Eisenberg ML, Lamb DL, Sandlow JI, Sokol RZ, Spandorfer SD,
1102 Tanrikut C, et al. Diagnosis and treatment of infertility in men: AUA/ASRM guideline part I. *Fertil Steril* 2021;**115**,
1103 54–61 https://doi.org/10.1016/j.fertnstert.2020.11.016
1104 Sironen A, Shoemark A, Patel M, Loebinger MR, Mitchison HM. Sperm defects in primary ciliary dyskinesia and
1105 related causes of male infertility. *Cell Mol Life Sci* 2020;77:2029-2048 https://doi.org/10.1007/s00018-019-
1106 03389-7
1107 Smith CEL, Lake ARV, Johnson CA. Primary Cilia, Ciliogenesis and the Actin Cytoskeleton: A Little Less Resorption,
1108 A Little More Actin Please. *Front Cell Dev Biol* 2020;8:622822 https://doi.org/10.3389/fcell.2020.622822
1109 Supernat A, Vidarsson OV, Steen VM, Stokowy T. Comparison of three variant callers for human whole genome
1110 sequencing. *Sci Rep* 2018;**8**:17851 https://doi.org/10.1038/s41598-018-36177-7
1111 Szklarczyk D, Gable AL, Lyon D, Junge A, Wyder S, Jaie Huerta-Cepas J, Simonovic M, Doncheva NT, Morris JH,
1112 Bork P et al. STRING v11: protein-protein association networks with increased coverage, supporting functional
1113 discovery in genome-wide experimental datasets. *Nucleic Acid Res* 2019;**47**:D607-D613
1114 https://doi.org/10.1093/nar/gky1131
1115 Tan JHL, Wollmann H, van Pelt AMM, Kaldis P, Messerschmidt DM. Infertility-Causing Haploinsufficiency Reveals
1116 TRIM28/KAP1 Requirement in Spermatogonia. *Stem Cell Rep* 2020;**14**:818-827
1117 https://doi.org/10.1016/j.stemcr.2020.03.013
1118 Touré A, Martinez G, Kherraf ZE, Cazin C, Beurois J, Arnoult C, Ray PF, Coutton C. The genetic architecture of
1119 morphological abnormalities of the sperm tail. *Hum Genet* 2021;**140**:21-42 https://doi.org/10.1007/s00439-020-
1120 02113-x

1121 Tourmente M, Villar-Moya P, Rial E, Roldan ER. 2015 Differences in ATP generation via glycolysis and oxidative
1122 phosphorylation and relationships with sperm motility in mouse species. J Biol Chem 2015;290:20613–20626
1123 https://doi.org/10.1074/jbc.M115.664813
1124 Tunyasuvunakool K, Adler J, Wu Z, Green T, Zielinski M, Žídek A, Bridgland A, Cowie A, Meyer C, Laydon A, et al.
1125 Highly accurate protein structure prediction for the human proteome. *Nature* 2021;**596**:590-596
1126 https://doi.org/10.1038/s41586-021-03828-1
1127 UniProt, C. UniProt: a worldwide hub of protein knowledge. *Nucleic Acids Res* 2019;**47**:D506-D15
1128 https://doi.org/10.1093/nar/gky1049
1129 Valassina N, Brusco S, Salamone A, Serra L, Luoni M, Giannelli S, Bido S, Massimino L, Ungaro F, Mazzara PG, et
1130 al. Scn1a gene reactivation after symptom onset rescues pathological phenotypes in a mouse model of Dravet
1131 syndrome. *Nat Commun* 2022;**13**:161 https://doi.org/10.1038/s41467-021-27837-w
1132 Vander Borght M,Wyns C. Fertility and infertility: Definition and epidemiology. *Clin Biochem* 2018;**62**: 2-10
1133 Varadi M, Anyango S, Deshpande M, Nair S, Natassia C, Yordanova G, Yuan D, Stroe O, Wood G, Laydoet A et al.
1134 AlphaFold Protein Structure Database: massively expanding the structural coverage of protein-sequence space
1135 with high-accuracy models. *Nucleic Acids Res* 2022;**50**:D439-D444 https://doi.org/10.1093/nar/gkab1061
1136 von Mering C, Jensen LJ, Snel B, Hooper SD, Krupp M, Foglierini M, Jouffre N, Huynen MA, Bork P. STRING: known
1137 and predicted protein-protein associations, integrated and transferred across organisms. *Nucleic Acid Res*
1138 2005;**33**:D433-443 https://doi.org/10.1093/nar/gki005
1139 Wagner K, Unger L, Salman MM, Kitchen P, Bill RM, Yool AJ. Signaling Mechanisms and Pharmacological
1140 Modulators Governing Diverse Aquaporin Functions in Human Health and Disease. *Int J Mol Sci* 2022;**23**:1388
1141 https://doi.org/10.3390/ijms23031388
1142 Wang C, Gu Y, Zhang K, Xie K, Zhu M, Dai N, Jiang Y, Guo X, Liu M, Dai J, et al. Systematic identification of genes
1143 with a cancer-testis expression pattern in 19 cancer types. *Nat Commun* 2016;**7**:10499
1144 https://doi.org/10.1038/ncomms10499
1145 Wertheimer E, Krapf D, de la Vega-Beltran, Sánchez-Cárdenas C, Navarrete F, Haddad D, Escoffier J, Salicioni AM,
1146 Levin LR, Buck J, Mager J, et al. Compartmentalization of distinct cAMP signaling pathways in mammalian sperm.
1147 *J Biol Chem* 2013;**288**:35307-35320 https://doi.org/10.1074/jbc.M113.489476
1148 WHO 2020: https://www.who.int/news-room/fact-sheets/detail/infertility

1149 Wilson KS, Gonzalez O, Dutcher SK, Bayly PV. Dynein-deficient flagella respond to increased viscosity with
1150 contrasting changes in power and recovery strokes. *Cytoskeleton (Hoboken)* 2015;**72**:477-490
1151 https://doi.org/10.1002/cm.21252
1152 Wirschell M, Olbrich H, Werner C, Tritschler D, Bower R, Sale WS, Loges NT, Pennekamp P, Lindberg S, Stenram
1153 U, et al. The nexin-dynein regulatory complex subunit DRC1 is essential for motile cilia function in algae and
1154 humans. *Nat Genet* 2013;45:262-268 https://doi.org/10.1038/ng.2533
1155 Wyrwoll MJ, Temel SG, Nagirnaja L, Oud MS, Lopes AM, van der Heijden GW, Heald JS, Rotte N, Wistuba J,Marius
1156 Wo¨ste M et al. Bi-allelic Mutations in M1AP Are a Frequent Cause of Meiotic Arrest and Severely Impaired
1157 Spermatogenesis Leading to Male Infertility. *Am J Hum Genet* 2020;107:342–351
1158 https://doi.org/10.1016/j.ajhg.2020.06.010
1159 Xavier MJ, Salas-Huetos A, Oud MS, Aston KI, Veltman JA. Disease gene discovery in male infertility: past, present
1160 and future. *Hum Genet* 2021;140:7-19 https://doi.org/10.1007/s00439-020-02202-x
1161 Xu W, Zhang Y, Qin D, Gui Y, Wang S, Du G, Yang F, Li L, Yuan S, Wang M, et al. Transcription factor-like 5 is a
1162 potential DNA- and RNA-binding protein essential for maintaining male fertility in mice. *J Cell Sci*
1163 2022;**135**:jcs259036 https://doi.org/10.1242/jcs.259036
1164 Xue M, Xue M, Fang Y, Sun G, Zhuo W, Zhong J, Qian C, Wang L, Wang L, Si J, Shujie Chen. IGFBP3, a transcriptional
1165 target of homeobox D10, is correlated with the prognosis of gastric cancer. *PLoS One* 2013;**8**:e81423
1166 https://doi.org/10.1371/journal.pone.0081423
1167 Yang J, Yan R, Roy A, Xu D, Poisson J, Zhang Y. The I-TASSER Suite: protein structure and function prediction. *Nat*
1168 *Methods 2015;***12;**7-8 https://doi.org/10.1038/nmeth.3213
1169 Yang J, Zhang Y. I-TASSER server: new development for protein structure and function predictions. Nucleic *Acids*
1170 *Res* 2015;**43**:W174-181 https://doi.org/10.1093/nar/gkv342
1171 Yang LF, Yang F, Zhang FL, Xie YF, Hu ZX, Huang SL, Shao ZM, Li DQ. Discrete functional and mechanistic roles of
1172 chromodomain Y-like 2 (CDYL2) transcript variants in breast cancer growth and metastasis. *Theranostics*
1173 2020;**10**:5242-5258 https://doi.org/10.7150/thno.43744
1174 Yin, M., O'Neil LAJ. The role of the electron transport chain in immunity. *FASEB J* 2021;**35**:e21974
1175 https://doi.org/10.1096/fj.202101161R

1176 Yuan J, Li X, Zhang G, Cheng W, Wang W, Lei Y, Ma Q, Song G. USP39 mediates p21-dependent proliferation and
1177 neoplasia of colon cancer cells by regulating the p53/p21/CDC2/cyclin B1 axis. *Mol Carcinog*enesis 2021;**60**:265-
1178 278 https://doi.org/10.1002/mc.23290
1179 Zhan K, Liu R, Tong H, Gao S, Yang G, Hossain A, Li T, He W. Fetuin B overexpression suppresses proliferation,
1180 migration, and invasion in prostate cancer by inhibiting the PI3K/AKT signaling pathway. *Biomed Pharmacother*
1181 2020;**131**:110689 https://doi.org/10.1016/j.biopha.2020.110689
1182 Zhang J, Liu S, Zhang D, Ma Z, Sun L. Homeobox D10, a tumor suppressor, inhibits the proliferation and migration
1183 of esophageal squamous cell carcinoma. *J Cell Biochem* 2019;**120**:13717-13725
1184 https://doi.org/10.1002/jcb.28644
1185 Zhang Z, Miao J, Wang Y. Mitochondrial regulation on spermatogenesis. Reproduction 2022;**163**:R55-R69
1186 https://doi.org/10.1530/REP-21-0431
1187 Zhao Y, Zhang B, Lei Y, Sun J, Zhang Y, Sen Yang S, Zhang X. Knockdown of USP39 induces cell cycle arrest and
1188 apoptosis in melanoma. *Tumour Biol* 2016;**37**:13167-13176 https://doi.org/10.1007/s13277-016-5212-x
1189 Zorrilla M, Yatsenko AN. The Genetics of Infertility: Current Status of the Field. *Curr Genet Med Rep* 2013;1:247–
1190 260 DOI 10.1007/s40142-013-0027-1

1191

1192

1193

1194

1195

1196 **Figures**

1197

1198 **Figure 1: Characteristics of *Tcte1* gene. A** Putative homologs of *Tcte1* gene conserved in Bilateria, according to
1199 HomoloGene (8434), including collation of proteins and their conserved domains; **B** Sequence alignement
1200 between human, mouse and rat; **C** NCBI Gene schematic representation of *Tcte1* gene in *Mus musculus*.

1201

1202 **Figure 2: Characteristics of *Tcte1* mice knockout. A** Schematic representation of gRNA localization in
1203 CRISPR/Cas9 KO creation; **B** Relative expression of *Tcte1* gene in wild type (WT), hetero- $^{(+/-)}$ and homozygous
1204 mice $^{(-/-)}$ (Real-time PCR); **** $p<0.0001$, ** $p<0.01$; **C** Example of genotyping result. Lane 1 – 1kb marker

1205 (GeneRuler), lanes 2, 3 – wild type (WT), lanes 4, 5 – hetero- $^{(+/-)}$, and lanes 6, 7 – homozygous mice $^{(-/-)}$; lanes: 2,
1206 4, 6 identified the lack (0 bp) or presence of mutation (630 bp), lanes: 3, 5, 7 differentiated hetero- (658 bp) and
1207 homozygotes (0 bp).
1208
1209 **Figure 3: Reproductive potential of KO *Tcte1* mice.** Mating combinations and their results including: time of
1210 breeding, number of litters and pups, number of male and female pups, and genotypes observed in pups of each
1211 combination. **A** Mean time: from mating to 1st pedigree, and between particular litters; **B** Ratio of males and
1212 females per litter in each mating combination; **C** Frequency of males and females and their genotype observed
1213 each mating combination; left panel: according to sex of pups; right panel: according to mating combinations; **D**
1214 Ratio of males and females per litter and their genotype observed each mating combination.
1215 *** $p < 0.0001$, ** $0.0001 < p < 0.01$, * $0.01 < p < 0.05$
1216
1217 **Figure 4: Characteristics of *Tcte1* wild type (WT), hetero- $^{(+/-)}$ and homozygous mice $^{(-/-)}$. A** Histopathology of
1218 testes and epididymises (caput); staining: Masson-Goldner protocol; microscope: Leica DM5500, objective 63×,
1219 magnification 630×; **B** Comparison of body mass, testis weight and size, and epididymis length, followed by gross
1220 morphology of gonads; **C** Sperm parameters: concentration, motility and morphology comparison; statistical
1221 marks indicated differences according to WT animals; **D** Frequency of morphological defects according to three
1222 part of the spermatozoa; **E** Examples of main sperm morphological abnormalities found (all abnormalities
1223 observed available in Supplementary file 7); **F** Comparison of the mean length of: sperm tail, midpiece and ratio
1224 tail:midpiece; *** $p < 0.0001$, ** $0.0001 < p < 0.01$, * $0.01 < p < 0.05$
1225
1226 **Figure 5: RNAseq results of changes in gene expression level found in testes of KO *Tcte1*$^{+/-}$ and *Tcte1*$^{-/-}$ mice vs.**
1227 **control (WT).** Volcano plots: black dots indicated all analyzed genes within the genome, red dots represented
1228 genes with significantly changed expression level (followed by the heatmap and the table). Filtering criteria: p
1229 val <0.05, log ratio >1 or <-1 (adequate to fold change value of 2 (expression level increased) or 0.5 (expression
1230 level decreased)), expression level >8. nd – no data concerning function or disease.
1231

1232 **Figure 6: STRING analyzis of potential interactions between proteins with observed differences in gene**
1233 **expression level in RNAseq for mouse testis of the KO model for *Tcte1* gene.** Genes revealed in RNAseq were
1234 bracketed. (STRING database, 24th Feb 2021).
1235
1236 **Figure 7: Immunolocalization of the nexin-dynein regulatory complex (N-DRC) proteins: Tcte1 (Drc5), Drc7,**
1237 **Fbxl13 (Drc6), and Eps8l1 (Drc3) within mouse sperm cells. A.** Localization of Tcte1 in spermatozoa from wild
1238 type (WT), hetero- ($^{+/-}$) and homozygous ($^{-/-}$) animals; **B.** Localization of other proteins (Drc7, Fbxl13, Eps8l1)
1239 building the nexin-dynein regulatory complex (N-DRC), responsible for coordination of the dynein arm activity
1240 and stabilization of the doublet microtubules attachment; wild type (WT) spermatozoa. Antibodies: primary (all
1241 anti-rabbit 1:100; Biorbyt, UK): Tcte1 (orb357083); Drc7 (orb58695); Fbxl13 (orb678278); Eps8l1 (orb382538);
1242 secondary: goat anti-rabbit-AF594 conjugated, 1:500, ab150160, Abcam, UK. Fluorescent microscope: Leica
1243 DM5500, filters – DAPI, TxR, FITC, BGR, magnification 630× (with immersion); software: LASX or CytoVision. Bar
1244 represents 10 μm.
1245
1246 **Figure 8: ATP level in wild type (WT), heterozygous ($^{+/-}$) and homozygous ($^{-/-}$) *Tcte1* mice.** Measurement done
1247 in two time points (0 and +60 min.) showed decrease of approximately 35% of luminescence in all three groups.
1248 Mean measured values in homozygous group were approximately 2.4-fold lower. Dots – particular animals; long
1249 dash – mean value for the group; short dashes – standard deviation; RLU – relative luminescence unit. ***
1250 $p<0.0001$, ** $0.0001 < p < 0.01$.
1251
1252 **Figure 9: Immunolocalization of caspase 3 within mouse testicular tissue of KO *Tcte1* model**. Caspase 3 is one
1253 of the apoptotic indicators becuase of its engagement in the induction, transduction, and amplification of
1254 intracellular apoptotic signals. Caspase 3 signals were found only on spermatogonia in all three genotypes
1255 evaluated (wild type (WT), hetero- ($^{+/-}$) and homozygous ($^{-/-}$)). No differences between the level of fluorescent
1256 signals were found between evaluated mouse genotypes, indicating similar level of apoptosis. Antibodies:
1257 primary (1:100) rabbit anti-Casp3 (Biorbyt, UK); secondary (1:500): goat anti-rabbit-AF594 conjugated
1258 (ab150160, Abcam, UK). Fluorescent microscope: Leica DM5500, filters – DAPI, TxR, magnification 630× (with
1259 immersion); software: LASX. Bar represents 5 μm. Analysed in 3 independent males per zygosity, on 15-20
1260 tubules each.

1261

1262 **Figure 10: Homology modeling of TCTE1. A** Secondary structure diagrams and associated confidence schema
1263 generated by I-TASSER [46,47,48], Phyre2[45], and AlphaFold [49,50] intensive mode. Positions of amino acids
1264 of interest are indicated. Green, predicted unstructured regions; yellow rectangles, predicted α-helices; orange
1265 arrows and arrowheads, predicted β–strands. Confidence scale ranges from white to cyan, with the probability
1266 of the secondary structure increasing with increasing intensity of cyan; **B** Cartoon diagram of homology model
1267 of human TCTE1 generated by AlphaFold with residues of interest shown as spheres and labeled. N, amino
1268 terminus; C, carboxy terminus; **C-F** Zoomed views of indicated residues and mutations: **C** Ile-125 resides deep
1269 within a hydrophobic pocket, which would be disturbed upon substitution with arginine; **D** Mutation R133C
1270 would impact the hydrogen bond interactions that organize the architecture of the globular domain N-terminal
1271 to the tandem leucine-rich repeats; **E** Mutation of Glu-157 to alanine would destabilize the charge of the surface
1272 of this globular region, likely leading to unfolding; **F** Gly-350 allows for the compact interactions of tandem α-
1273 helices of the LRR. Depending on the rotamer it adopted, a serine side chain in this position would sterically clash
1274 with residues D321, A324, or V346 in the neighboring helix.

1275

1276 **Figure 11: Summary of findings revealed for abnormal sperm tail beating in mouse knockout model of *Tcte1***
1277 **gene, a component of the N-DRC complex in sperm tail.** Three major groups of factors required for proper sperm
1278 tail beating were marked with bold colour arrows (green, yellow and blue). Documented connections (solid grey
1279 arrows) revealed on the basis of: RNAseq data for testis tissues, protein *in silico* predictioning for mutated Tcte1
1280 protein, and measurements of ATP level and sperm cell components in mouse spermatozoa. Unresolved possible
1281 linkages (cause/effect) marked with question (?) mark.

1282

1283

1284

1285

1286

1287

1288

1289

1308 Figure 1

A

species	gene symbol	Gene ID/ NCBI	UniProt	Indentity (%)		conserved domains
				protein	DNA	Leucine-rich repeats (LRRs), cd00116 Leucine-rich repeats (LRRs), cl15309 CemA family (cl03855)
H. sapiens	*TCTE1*	202500	Q5JU00			NP_872345.2, 501 aa
vs.						
P. troglodytes	*TCTE1*	462732	H2QT36	99.2	99.2	XP_518509.2, 501 aa
M. mulatta	*TCTE1*	702738	F7CLN3	97.0	96.9	XP_001099848.1, 501 aa
C. lupus	*TCTE1*	609664	-	85.4	87.0	XP_852058.1, 501 aa
B. taurus	*TCTE1*	523600	-	77.3	80.3	XP_002697348.1, 246 aa
M. musculus	*Tcte1*	21645	A6H639	77.3	77.5	NP_038716.2, 498 aa
R. norvegicus	*Tcte1*	316242	D3ZQW5	78.0	78.0	NP_001101676.1, 498 aa
G. gallus	*TCTE1*	421437	-	63.8	66.8	XP_004935446.1, 457 aa
X. tropicalis	*tcte1*	100487694	-	57.6	63.5	XP_002942200.1, 460 aa
D. rerio	*tcte1*	100331698	I3IS38	55.5	61.0	XP_002667399.3, 448 aa
D. melanogaster	*CG14325*	42123	Q9VEH4	31.6	43.6	NP_650641.2, 460 aa
A. gambiae	*AgaP_AP002751*	1273219	Q7QCP9	28.3	45.5	XP_312174.4, 430 aa

B

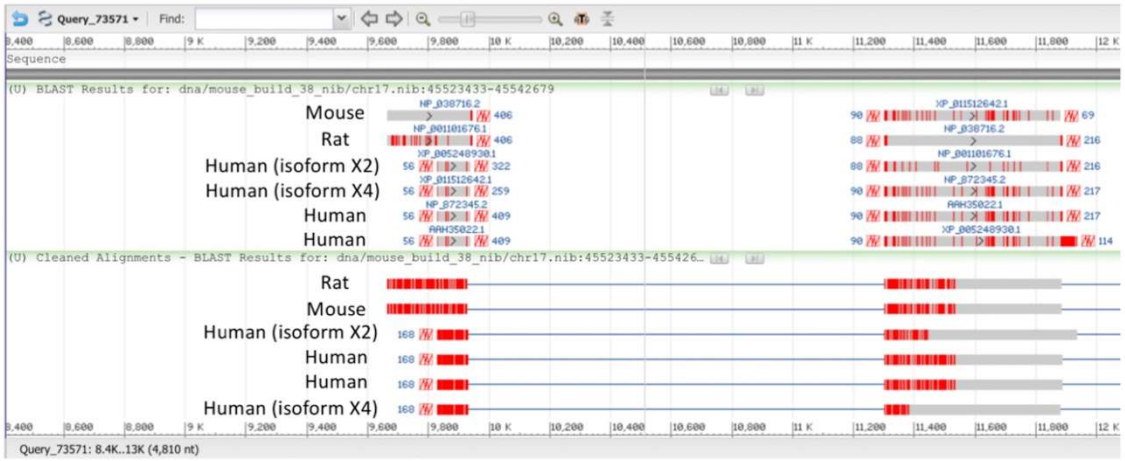

C

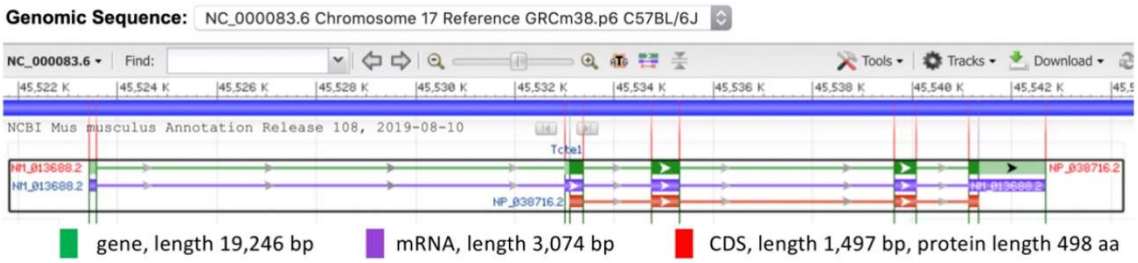

1309

1310

1311

1312

1313

1314

1315

1316

1317

1318 Figure 2

1319

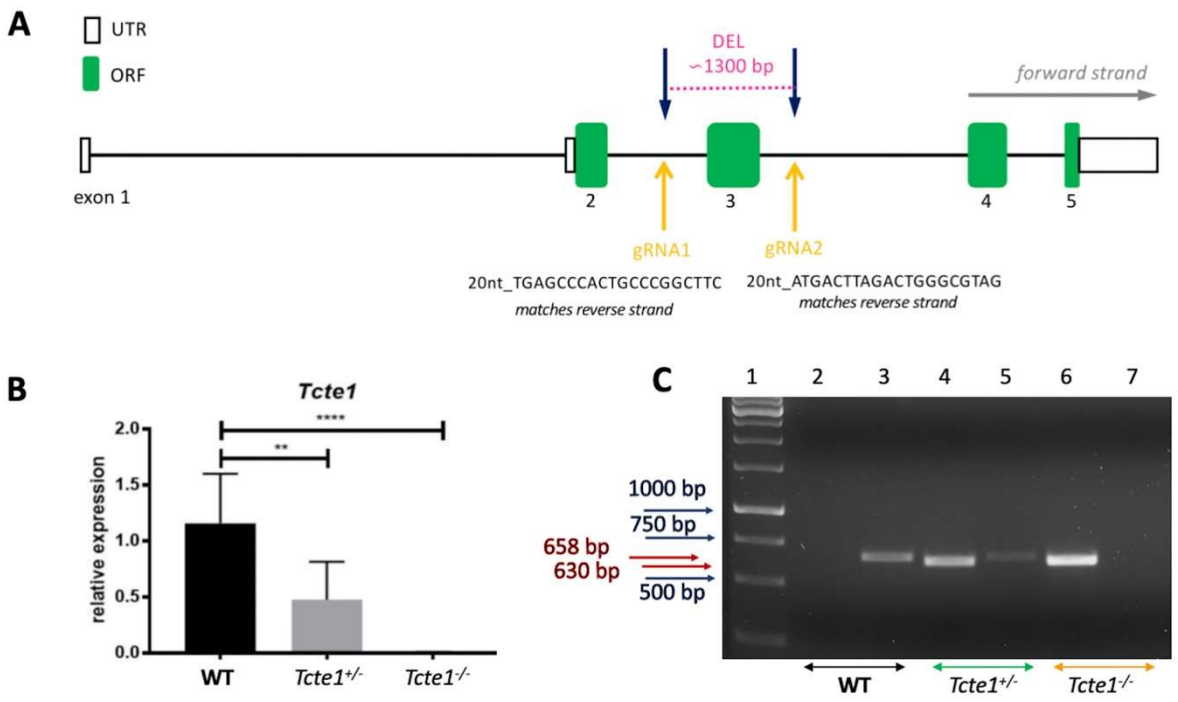

1320

1321

1322

1323

1324

1325

1326

1327

1328

1329

1330

1331

1332

1333

1334

1335

1336

1337

1338

1339

1340

1341 Figure 3

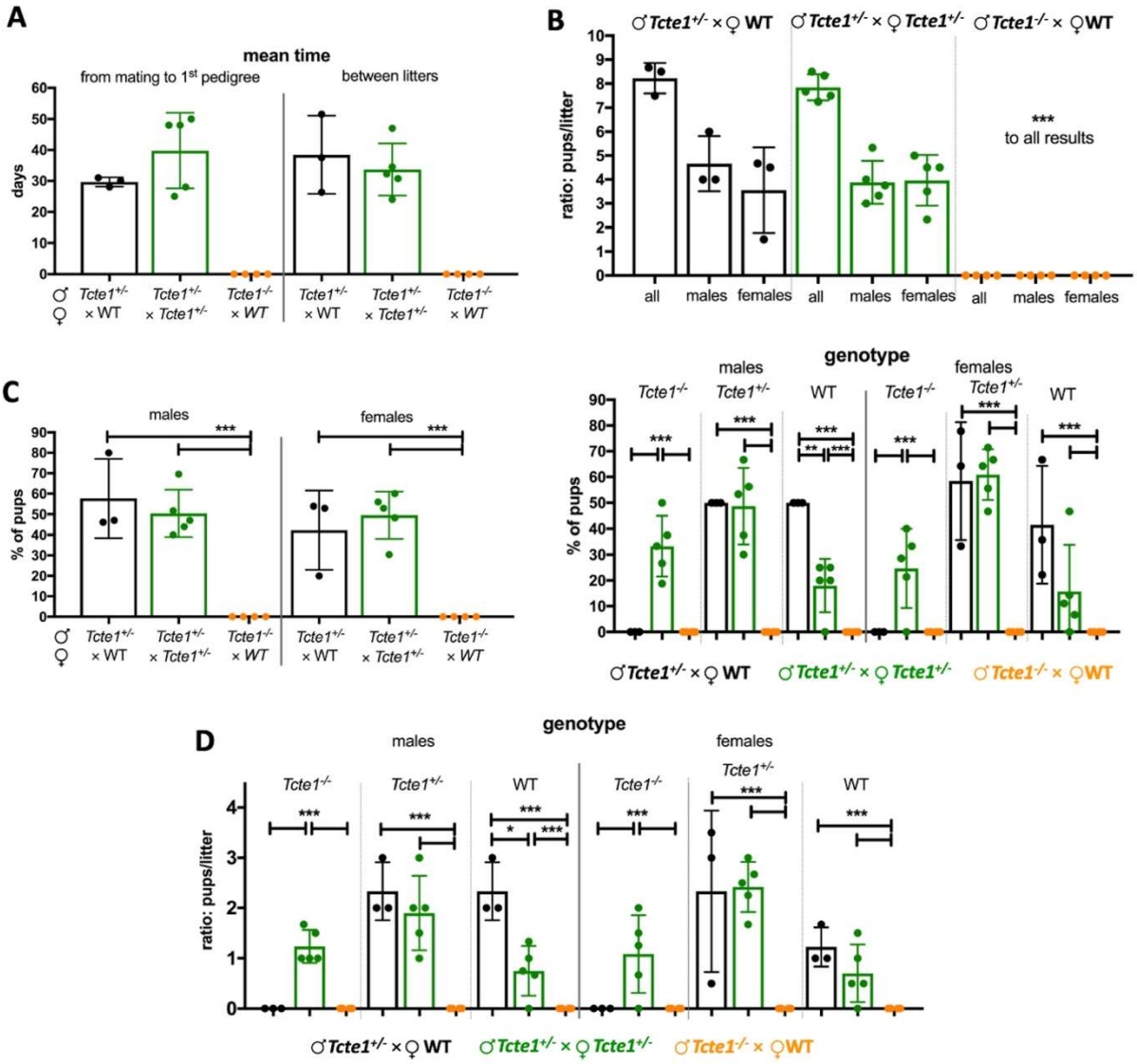

1342

1343

1344

1355 Figure 4

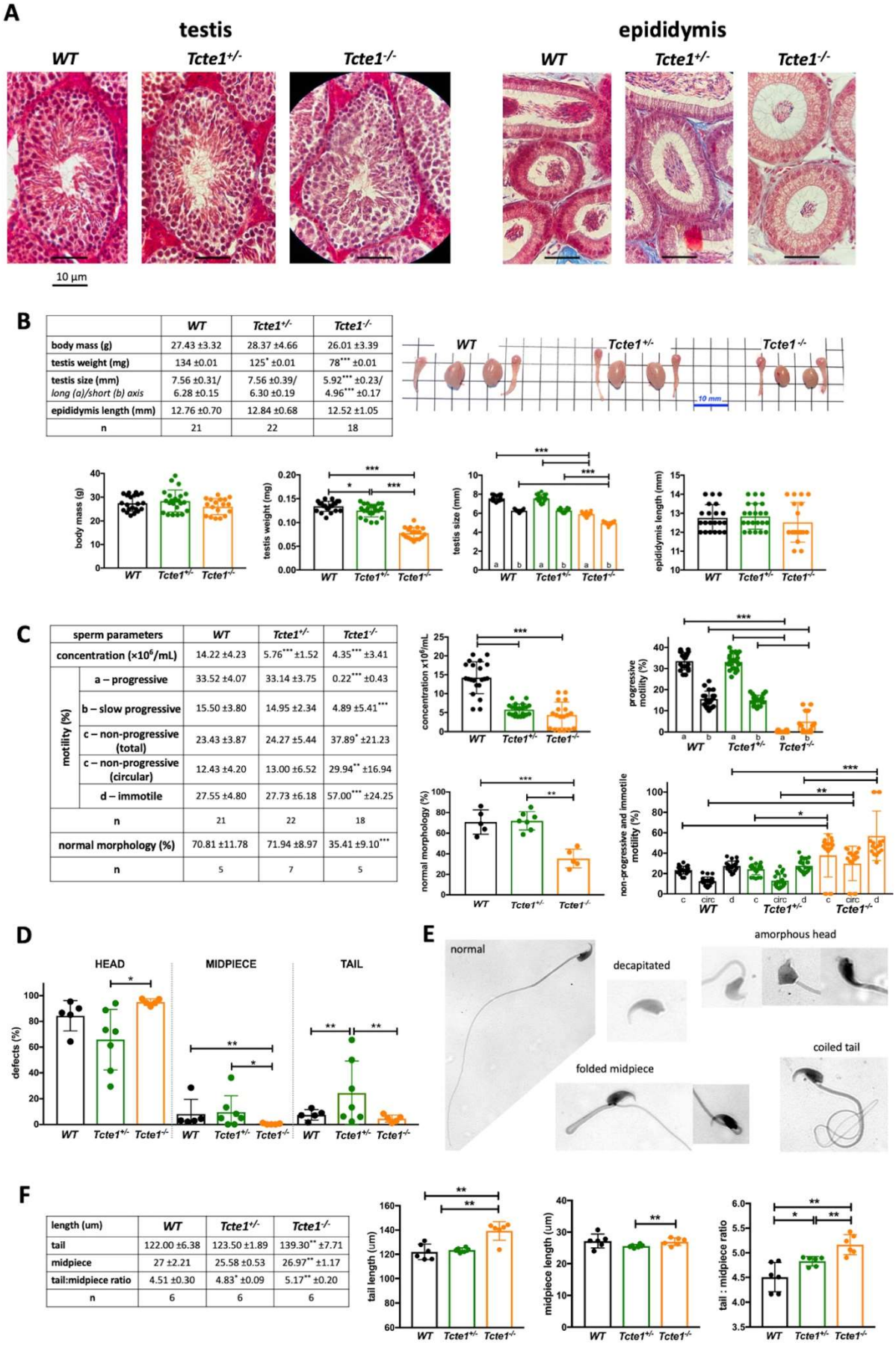

	WT	Tcte1+/-	Tcte1-/-
body mass (g)	27.43 ±3.32	28.37 ±4.66	26.01 ±3.39
testis weight (mg)	134 ±0.01	125* ±0.01	78*** ±0.01
testis size (mm) *long (a)/short (b) axis*	7.56 ±0.31/ 6.28 ±0.15	7.56 ±0.39/ 6.30 ±0.19	5.92*** ±0.23/ 4.96*** ±0.17
epididymis length (mm)	12.76 ±0.70	12.84 ±0.68	12.52 ±1.05
n	21	22	18

sperm parameters		WT	Tcte1+/-	Tcte1-/-
concentration (×10^6/mL)		14.22 ±4.23	5.76*** ±1.52	4.35*** ±3.41
motility (%)	a – progressive	33.52 ±4.07	33.14 ±3.75	0.22*** ±0.43
	b – slow progressive	15.50 ±3.80	14.95 ±2.34	4.89 ±5.41***
	c – non-progressive (total)	23.43 ±3.87	24.27 ±5.44	37.89* ±21.23
	c – non-progressive (circular)	12.43 ±4.20	13.00 ±6.52	29.94** ±16.94
	d – immotile	27.55 ±4.80	27.73 ±6.18	57.00*** ±24.25
n		21	22	18
normal morphology (%)		70.81 ±11.78	71.94 ±8.97	35.41 ±9.10***
n		5	7	5

length (um)	WT	Tcte1+/-	Tcte1-/-
tail	122.00 ±6.38	123.50 ±1.89	139.30** ±7.71
midpiece	27 ±2.21	25.58 ±0.53	26.97** ±1.17
tail:midpiece ratio	4.51 ±0.30	4.83* ±0.09	5.17** ±0.20
n	6	6	6

1356 Figure 5

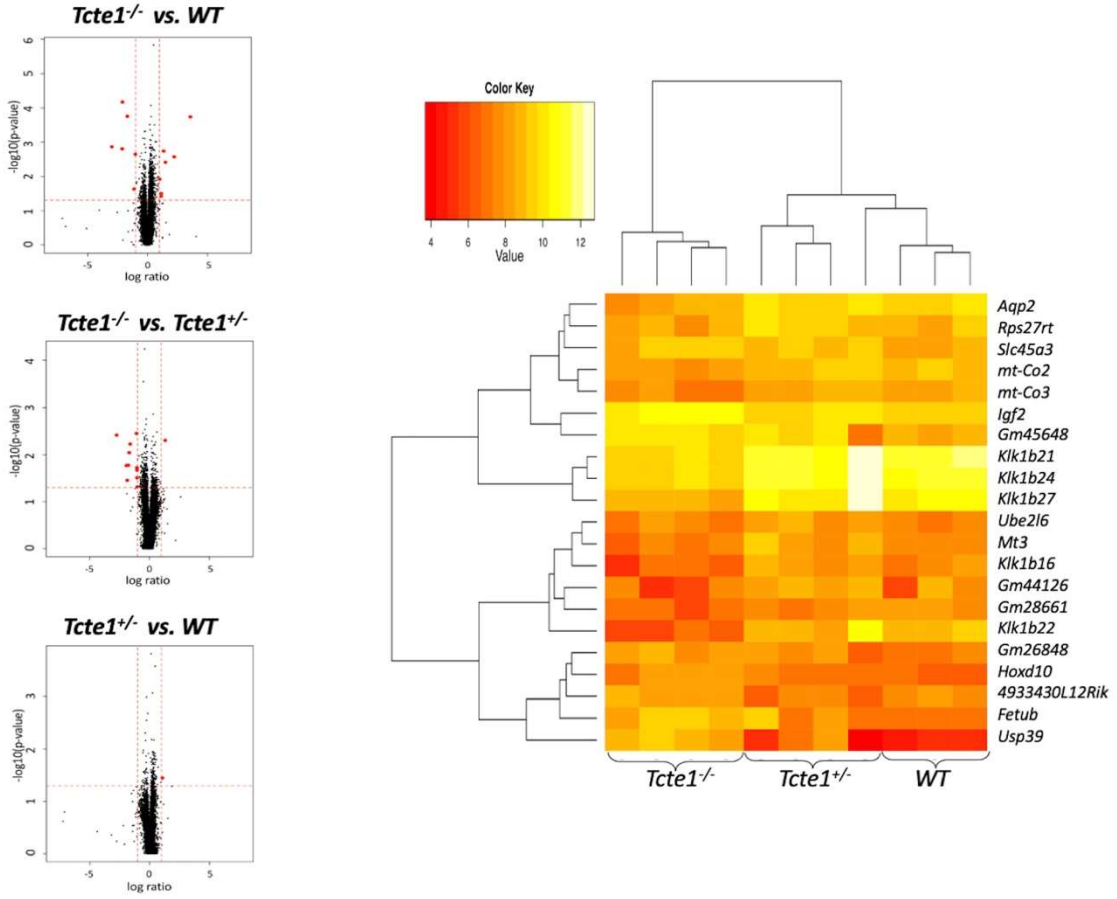

gene symbol	gene ID /NCBI	gene type	fold change			known function/characteristics/disease
			Tcte1$^{-/-}$ vs. WT	*Tcte1*$^{-/-}$ vs. *Tcte1*$^{+/-}$	*Tcte1*$^{+/-}$ vs. WT	
Klk1b27	16619	protein coding	0.2305	0.2937	-	degradation of extracellular matrix proteins in the interstitial area
Klk1b21	16616	protein coding	0.2333	0.2626	-	surrounding the Leydig cells of the adult mouse testis,
Klk1b24	16617	protein coding	0.3101	0.3102	-	seminal liquefaction
Klk1b16	16615	protein coding	-	0.3277	-	seminal liquefaction
Klk1b22	13646	protein coding	0.1266	0.1494	-	neurons' differentiation
mt-Co2	17709	protein coding	0.4966	0.4734	-	mitochondrial cytochrome oxidase subunit, asthenozoospermia, cancer
mt-Co3	17710	protein coding	-	0.4859	-	diabetes, deafness, apoptosis
Fetub	59083	protein coding	4.6789	-	-	fertilization marker, sperm binding to *zona pellucida*, diabetes, coronary disease, inhibition and apoptosis of prostate cancer cells
Hoxd10	15430	protein coding	2.8503	-	-	prostate cancer, cell differentiation and morphogenesis
Igf2	16002	protein coding	2.0400	-	-	spermatogenesis, sex determination, testis development, infertility, sperm DNA damage, prostate cancer, apoptosis
Slc45a3	212980	protein coding	2.2164	-	-	prostate cancer, myelin maintenance
Usp39	28035	protein coding	12.0339	-	-	spliceosomal complex, prostate cancer, apoptosis, cytokinesis, mitotic spindle checkpoint, vascular remodeling
Gm28661	-	unprocessed pseudogene	0.4576	-	-	nd
Gm26848	-	protein coding	2.2287	-	-	nd (membrane trasporter-like protein in *D. sechellia*)
Gm45648	102637934	ncRNA	2.5642	-	-	nd (testis-restricted expression in mouse)
Aqp2	11827	protein coding	-	0.4813	-	spermatogenesis, female endometrium cycle, stress urinary incontinence
Mt3	17751	protein coding	-	0.4868	-	testis protection from cadmium, apoptosis, VEGF induction, retinal damage, Alzheimer disease
Rps27rt	100043813	protein coding	-	0.4842	-	ribosomal protein
Gm44126	-	protein coding (?)	-	0.2745	-	nd (suggested: UDP-glucuronic acid decarboxylase in mouse)
4933430L12Rik	71251	protein coding	-	2.5102	-	nd
Ube2l6	56791	protein coding	-	0.4969	2.1110	cancer, apoptosis, autophagy, obesity

Figure 6

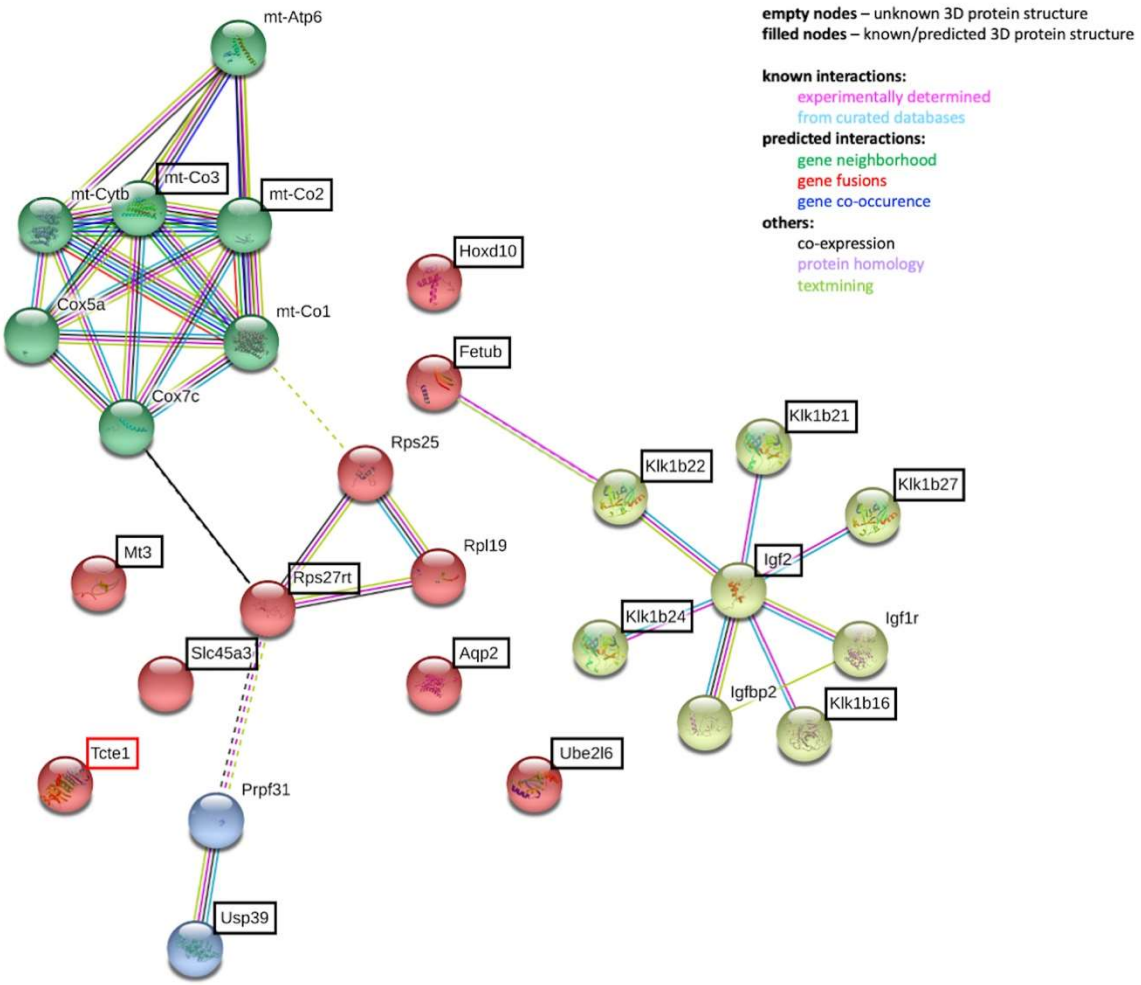
empty nodes – unknown 3D protein structure
filled nodes – known/predicted 3D protein structure
known interactions:
experimentally determined
from curated databases
predicted interactions:
gene neighborhood
gene fusions
gene co-occurence
others:
co-expression
protein homology
textmining
mt-Atp6
mt-Cytb
mt-Co3
mt-Co2
Cox5a
mt-Co1
Cox7c
Hoxd10
Fetub
Rps25
Rpl19
Mt3
Rps27rt
Slc45a3
Aqp2
Tcte1
Prpf31
Usp39
Ube2l6
Klk1b21
Klk1b22
Klk1b27
Igf2
Klk1b24
Igf1r
Igfbp2
Klk1b16

1373 Figure 7

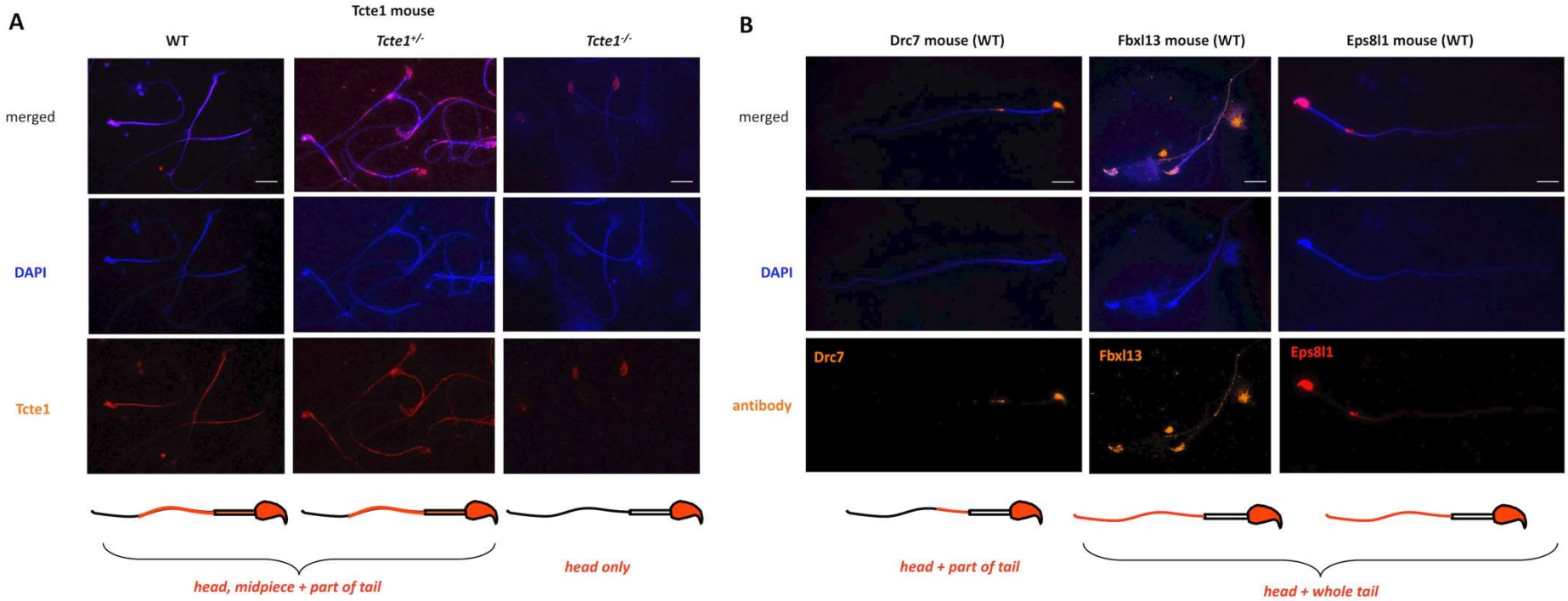

1374

1375

1376

1377

1378

1379

1382 Figure 8

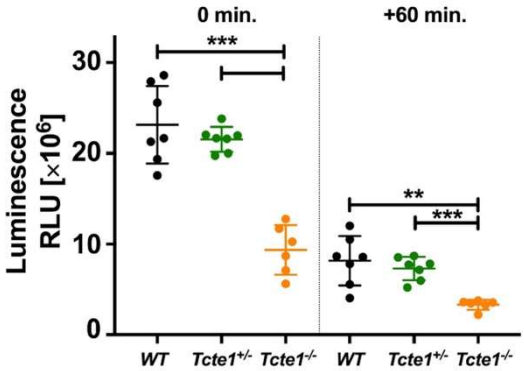

1383

1384

1385

1386

1387

1388

1389 Figure 9

1390

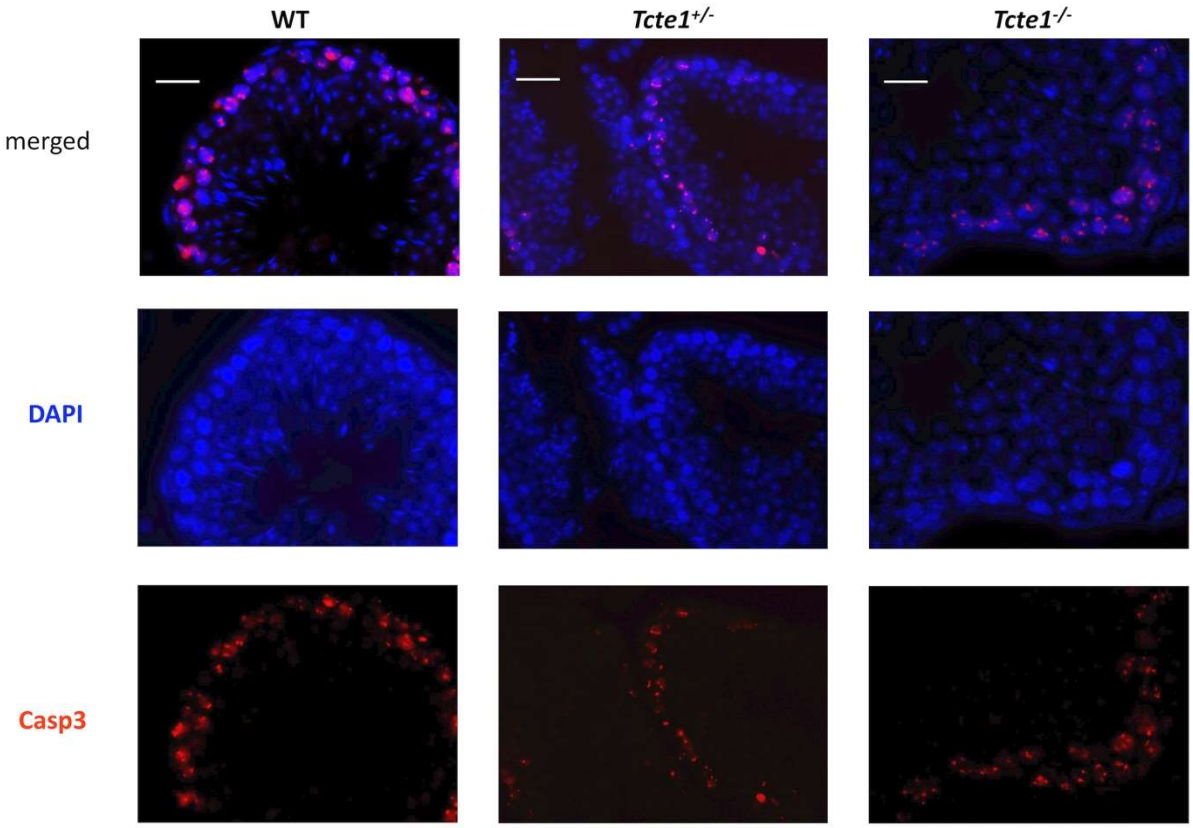

1391

1392

1393

1394

1395 Figure 10

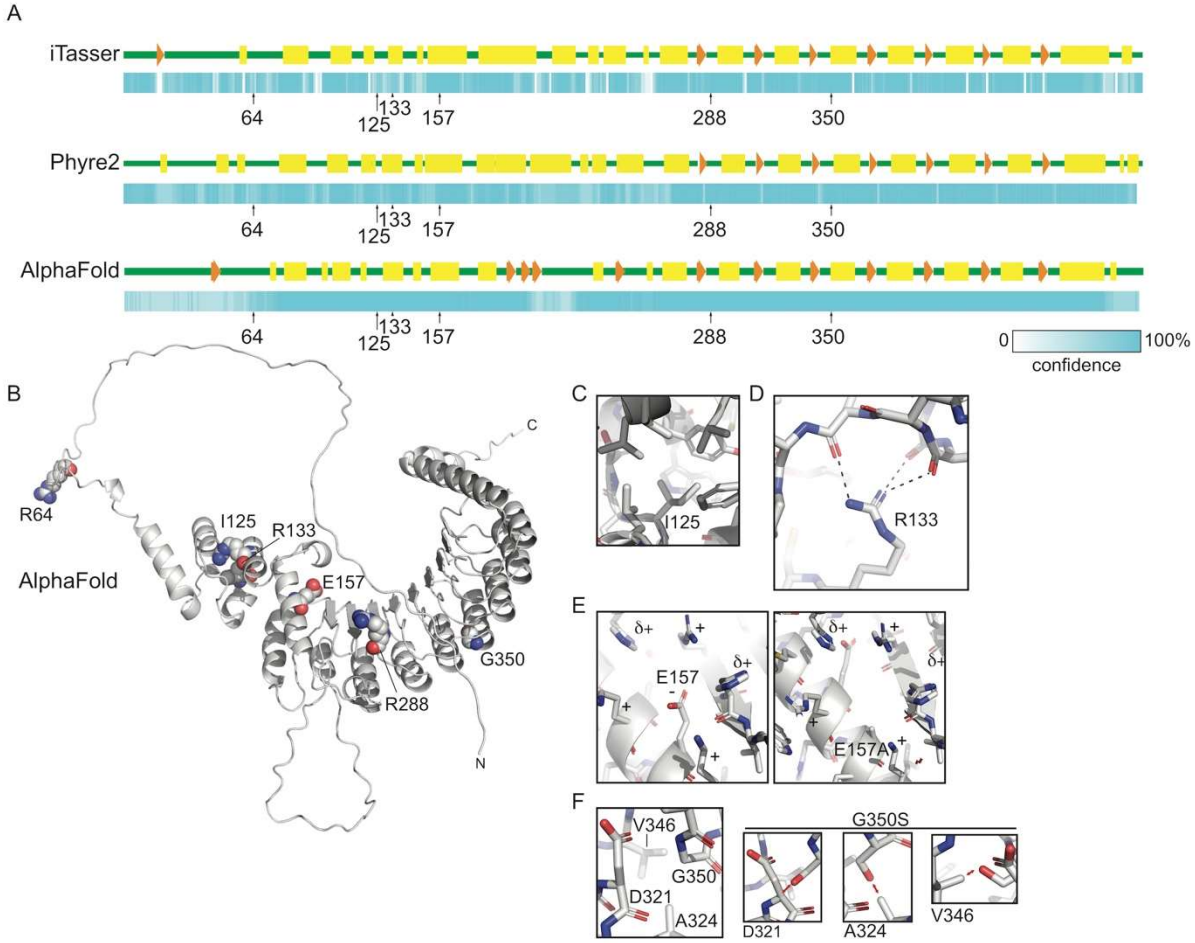

1396

1397

1398

1399

1400

1401

1402

1403

1404

1405

1406 Figure 11

1407

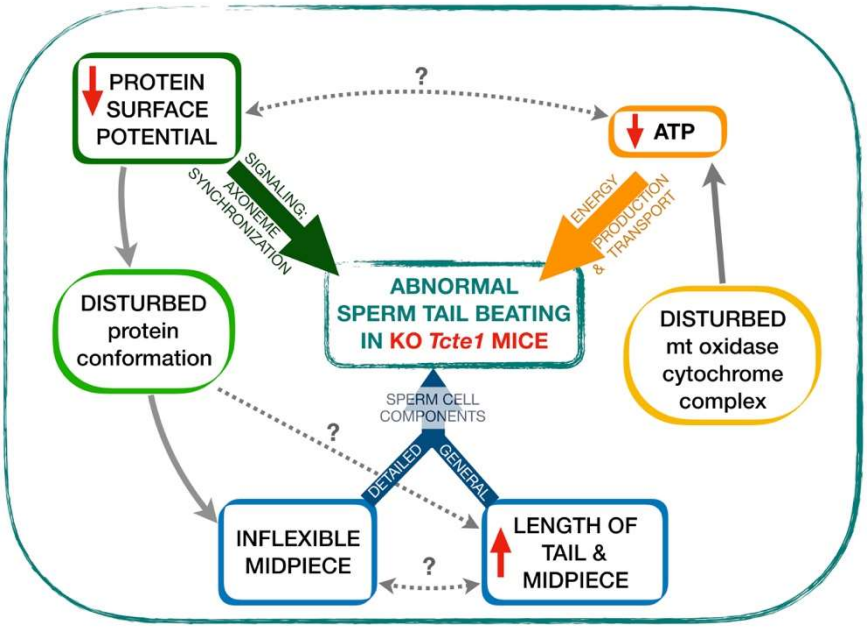

1408 **Table 1** Potentially disease-causing novel and ultrarare heterozygous *TCTE1* variants found in patients with disturbed spermatogenesis. Results obtained from screening of

1409 n=248 participants. Minor allele frequency data obtained from GnomAD v2.1.1.

1410 SOAs – severe oligoasthenozoospermia; NOA – non obstructive azoospermia; SCO – Sertoli Cell-Only syndrome; Crypto – cryptozoospermia; NMD – non mediated decay; NT

1411 – nucleotide; AA – amino acid; SNV – single nucleotide variant; PLoF – Loss of Function probability; rs – Reference SNP accession number; CADD – Combined Annotation

1412 Dependent Depletion tool

Sample ID	**Phetotype**	**origin**	**NT change**	**cDNA position**	**prediction**	**Mutation T@ster**	**GnomAD**	**rs**	**length of protein**	**CADD**	**position(s) of altered AA [HGVSp]**	**Polyphen/ Sift**
novel variants												
P52, P88, P105, P111, P161	SOAs	Poland	c.374T>G	cDNA.497T>G	disease causing	amino acid sequence changed; protein features (might be) affected; splice site changes	not found	-	normal	missense	p.Ile125Arg	unknown
P94	Crypto											
P149	NOA											
ultrarare variants (MAF <0.005)												

U13	NOA	USA	c.185G>A	cDNA.308G>A	disease causing	amino acid sequence changed	0.00007778	rs201144307	normal	missense	p.Arg62His	probably damaging/ deletorious
U17	NOA: meiotic arrest	USA	c.397C>T	cDNA.520C>T	disease causing	amino acid sequence changed; heterozygous in TGP or ExAC; protein features (might be) affected; splice site changes	0.001722	rs145304614	normal	missense	p.Arg133Cys	probably damaging/ deletorious
U50, U57, U117, U235	NOA	USA	c.470A>C	cDNA.593A>C	disease causing	amino acid sequence changed; heterozygous in TGP or ExAC; protein features (might be) affected; splice site changes	0.002681	rs45591736	normal	missense	p.Glu157Ala	probably damaging/ deletorious

U11	NOA: meiotic arrest	USA	c.862C>T	cDNA.985C>T	disease causing	NMD amino acid sequence changed; protein features (might be) affected; splice site changes	0.0002840	rs138414421	NMD	stop_gained	p.Arg288Ter	stopgain SNV; PLoF: high confidence
U76	NOA	USA	c.1048G>A	cDNA.1171G>A	disease causing	amino acid sequence changed; protein features (might be) affected; splice site changes	0.00006382	rs570334918	normal	missense	p.Gly350Ser	probably damaging/ deletorious

1413

1414 **Supplementary files legend**

1415

1416 **Supplementary File 1: Vectors used for knockout creation of Tcte1 gene.**

1417

1418 **Supplementary File 2: Real time PCR conditions used for determination of relative expression level of *Tcte1***

1419 **gene in mouse knockout animals.**

1420

1421 **Supplementary File 3: Reproductive potential of KO *Tcte1* mice.** Mating combinations and their results

1422 including: time of breeding, number of litters and pups, number of male and female pups, and genotypes

1423 observed in pups of each combination.

1424

1425 **Supplementary File 4: Genotyping protocol for *Tcte1* knockout model.**

1426

1427 **Supplementary File 5: Characteristics of antibodies used for N-DRC complex staining in mouse sperm.** Human

1428 antigen sequence identity between human and mouse orthologs was also shown (blast comparison; information

1429 from Biorbyt producer).

1430

1431 **Supplementary File 6: Schematic models of exon 3 deleted in KO mice. A** Tcte1 protein exon 3 (deleted in KO)

1432 prediction of 5 top models (software: I-TASSER). C-score is the confidence score of the prediction. C-score ranges

1433 [0-1], where a higher score indicates a more reliable prediction; TM-score is a measure of global structural

1434 similarity between query and template protein., RMSD - root-mean-square deviation of the average distance

1435 between the atoms. **B** The deletion sequence used for modeling, including exon 3 (yellow).

1436

1437 **Supplementary File 7: An example of circular type movement pathway of spermatozoa from *Tcte1*$^{-/-}$ male mice.**

1438

1439 **Supplementary File 8: An example of sperm cells motility in *Tcte1*$^{+/-}$ male mice.**

1440

1441 **Supplementary File 9: An example of sperm cells motility in *WT* male mice.**

1442

1443 **Supplementary File 10:** Detailed parameters of mouse sperm morphology. Statistically significant values: $p <$
1444 0.05; ns – statistically not significant ($p \geq 0.05$). For samples with normal distribution (positive Shapiro-Wilk
1445 normality test), t-test with Welch's correction was applied; for samples without normal distribution (midpiece
1446 and tail defects), Kolmogorov-Smirnoff test was applied (GraphPad Prism v. 7.0e). n=200 spermatozoa were
1447 analyzed per each mouse; for WT and *Tcte1*$^{-/-}$ n=5 animals were evaluated, while for *Tcte1*$^{-/+}$ the number of
1448 animals was n=7. Spermatozoa stained with the classic Papanicolau staining procedure. Bright field microscope:
1449 Leica DM5500, magnification 630x (with immersion), software: CytoVision.
1450
1451 **Supplementary File 11: STRING analyzis data for each gene with changed expression pattern in *Tcte1* KO mouse**
1452 **model.**
1453
1454 **Supplementary File 12: STRING analyzis of potential interactions between proteins with observed major**
1455 **differences in gene expression level in mouse testis of the homozygous *Tcte1* mice (Usp39, Fetub, Klk1b22).**
1456 According to genes revealed in RNAseq analysis (marked with arrows), two groups of interactions were formed
1457 for genes with highest expression changes (red arrows); (STRING database, 11th March 2021).
1458
1459 **Supplementary File 13: ATP measurement data obtained for KO Tcte1 male mice.** wt = wild type, het =
1460 heterozygous, ho - homozygous. RLU = relative luminescence unit.
1461
1462 **Supplementary File 14: Examples of potentially disease-causing rare heterozygous *TCTE1* variants found in**
1463 **patients with disturbed spermatogenesis.** Results obtained from screening of n=248 participants. **A** novel
1464 variant (Sanger sequencing); **B** ultra rare variants (WES).
1465
1466 **Supplementary File 15: The C-terminal region of TCTE1 was consistently modeled and fits well in published**
1467 **maps. A** Superposition of the cartoon representation of three models of human TCTE1 generated by Phyre2 [45]
1468 intensive (green) or fast mode (grey), I-TASSER [46,47,48] (yellow), and AlphaFold [49,50] (cyan). N- and C-termini
1469 are labeled. **B.** Manual docking of the model of full-length TCTE1 generated by AlphaFold in maps calculated from
1470 a cryo-electron tomography experiment performed on *C. reinhardtii* using nanogold to locate the C-terminus of
1471 DRC5 (EMD-20821) [23].